Journal of Materials Processing Tech. 305 (2022) 117586

Contents lists available at ScienceDirect

Journal of Materials Processing Tech.

journal homepage: www.elsevier.com/locate/jmatprotec

Review

A critical comparative review of cavitation peening and other surface peening methods

Hitoshi Soyama [a,*], Alexander M. Korsunsky [b]

[a] Department of Finemechanics, Tohoku University, 6-6-01 Aoba, Aramaki, Aoba-ku, Sendai 980-8579, Japan
[b] Department of Engineering Science, University of Oxford, Parks Road, Oxford OX1 3PJ, UK

ARTICLE INFO

Associate Editor: Adam Thomas Clare

Keywords:
Surface modification
Cavitation peening
Shot peening
Fatigue strength
Residual stress
Hardness
Surface roughness

ABSTRACT

Mechanical surface modification such as shot peening offer powerful enhancement of fatigue properties of metals and other materials. Cavitation usually causes surface damage in hydraulic machineries. However, careful selection of process parameters allowed developing an approach known as "cavitation peening." Its advantage is surface roughness increase is lower than in conventional shot peening as there are no solid collisions involved. As cavitation is a hydrodynamic phenomenon, an understanding of both fluid dynamics and materials science is required. Cavitation peening is distinguished from "water jet peening," in which water column impulse is used. Another flavor is "Submerged laser peening" that involves the use of a pulsed laser and can be considered a type of cavitation peening where cavitating bubbles are generated due to laser ablation. Ultrasound vibration, a popular method for generating cavitation for cleaning, has also been adapted for cavitation peening. The present comparative review presents key insights and achievements and addresses future directions that are required for advancing cavitation peening technology by considering the mechanisms of cavitation peening based on the reported data for water jet, pulsed laser, and ultrasonic cavitation peening. The data and methods are critically considered and summarized in comparison with shot peening. Strategic view of future challenges is presented.

1. Introduction

Mechanical surface modification by a family of processes such as shot peening can improve the fatigue strength and/or fatigue life of metallic materials by introducing compressive residual stress and work hardening. For example, Delosrios et al. (1995) demonstrated the effect of shot peening on the initiation and propagation of fatigue cracks. Torres and Voorwald (2002) evaluated the residual stress introduced by shot peening and its relaxation during fatigue. Guechichi and Castex (2006) proposed a method to predict the fatigue limit by considering the compressive residual stress introduced by shot peening. Zhou et al. (2018) considered the relaxation of compressive residual stress induced by shot peening during fatigue. Shot peening is also applied to additively manufactured (AM) metallic materials. Bagherifard et al. (2018) demonstrated properly enhancement for AM AlSi10Mg parts by shot peening, and Kahlin et al. (2020) demonstrated the improvement of fatigue strength of AM Ti6Al4V by shot peening. Bellows and Koster (1972) revealed that the fatigue limit decreased with an increase in surface roughness, while shot peening increased surface roughness by solid collisions. Miao et al. (2010) revealed the surface roughness as a function of the processing time of shot peening until 100% coverage was achieved. Bagherifard et al. (2012) investigated the surface roughness generated by shot peening using numerical and experimental analyses. Wu et al. (2020) showed the effect of shot peening coverage on the residual stress and surface roughness. Shot peening thus is indeed an effective method for improving the fatigue properties of metallic materials. However, there is a need to develop a peening method with less significant increase in the surface roughness. Cavitation peening has been proposed as a promising alternative that can reduce the increase in surface roughness in which impacts caused by bubble collapse are utilized to produce plastic deformation pits instead of shot collisions not involved in cavitation peening. Simply put, cavitation peening is a kind of shotless peening and has been called "cavitation shotless peening", a term coined by Soyama et al. (2002).

Cavitation peening is classified into three types according to the cavitation generation method: hydraulic cavitation using a water jet, laser cavitation using a pulsed laser, and ultrasonic cavitation using ultrasonic transducer. In the introduction, the history of each method is described, and an outline of the present review is revealed.

Cavitation impacts normally cause severe damage to hydraulic

* Corresponding author.
E-mail address: soyama@mm.mech.tohoku.ac.jp (H. Soyama).

https://doi.org/10.1016/j.jmatprotec.2022.117586
Received 21 December 2021; Received in revised form 24 March 2022; Accepted 31 March 2022
Available online 5 April 2022

machinery such as pumps and valves (Brennen, 1995). By considering the reversal of this idea, Soyama et al. (1996a) proposed that cavitation impacts around a submerged high-speed water jet introduced compressive residual stress into stainless steel, which Hirano et al. (1996) confirmed and applied to nuclear power plants to mitigate stress corrosion cracking (Saitou et al., 2003). Enomoto et al. (1996) introduced water jet peening, in which water column collision with the target was used to mitigate the stress corrosion cracking in nuclear power plant. Submerged high-speed water jet can peen the metallic material surfaces by "water jet peening" (momentum transfer) or by "cavitation peening" in which cavitation impacts are used. The peening mechanism and optimum conditions for both peening methods are completely distinct and different. Kamisaka and Soyama (2018) clearly demonstrated that cavitation peening can allow higher efficiency processing than water jet peening. In the present review the mechanisms of cavitation peening and water jet peening are explained, and a method of distinguishing between these modalities was proposed. Fig. 1 shows a typical aspect of an impinging submerged high-speed water jet with cavitation, that is, a cavitating jet. The flow direction is from the left to right, and the cloud of white bubbles correspond to cavitation. A pressurized water was continuously injected into the water, causing the cavitation cloud to be shed periodically, and to become a ring cavitation vortex seen at the target surface (Soyama, 2017).

The other type of shotless peening is "laser peening" that uses a pulses laser and can be classified into further two types. One method is a water-film type, in which a powerful laser (several J per pulse) is used with a film of water and a protective tape or coating on the target. Peyre et al. (1996) demonstrated the enhancement of the fatigue limit of aluminum alloy by laser peening of the water-film type compared to shot peening. The effective of service temperature on the tensile properties of commercial pure titanium treated by laser peening with silicon oil was reported by Lu et al. (2019), and tensile strength and ductility of titanium alloy manufactured by selective laser melting treated by laser peening with water film was also revealed by Lv et al. (2022). Wang et al. (2020) demonstrated the extension of fatigue life by laser peening and Lu et al. (2021) revealed the effect of laser peening on the hot corrosion behavior of the selected laser melted Ti6Al4V. The other method is a submerged type, in which the target is placed in water. Sano et al. (2006) revealed retardation of crack initiation and growth in austenitic stainless steel by submerged laser peening without protective coating, and Sano (2020) summarized the development of submerged laser peening, including mitigation of stress corrosion cracking in nuclear power plant. In both water-film type and submerged type, shockwaves are produced by ablation generated by the pulsed laser and trapped by the inertial force of water, causing plastic deformation of the target. Both laser peening methods are likely to use ablation to produce plastic deformation. Note that in the case of submerged laser peening, a bubble, which behaves like a cavitation bubble, is generated by a negative pressure wave after the shock wave induced by the laser ablation. In the present paper, the bubble caused by the pulsed laser is called "laser cavitation". Sasoh et al. (2005) reported that the amplitude of the pressure wave induced by laser ablation was larger than that of laser cavitation, when the pressure wave in water was measured by a submerged shockwave sensor. However, when the impact passing through the target was measured using a polyvinylidene fluoride (PVDF) sensor, which was originally developed to evaluate cavitation impacts by Soyama, the impact of laser cavitation collapse was greater than that of laser ablation (Soyama, 2019). Ren et al. (2018) investigated the mechanical effect of laser cavitation of aluminum alloys, and Gu et al. (2021a) reported the introduction of compressive residual stress and work hardening by laser cavitation peening. Soyama (2021a) revealed that the submerged laser peening intensity was proportional to the volume of laser cavitation and laser cavitation peening improved the fatigue strength of the welded part. In other words, submerged laser peening is a type of cavitation peening using laser cavitation. Thus, cavitation peening using a pulsed laser is also summarized in the present review. Fig. 2 shows the laser ablation and laser cavitation of the submerged laser peening in one picture by double exposure photography. The pulsed laser was irradiating from the left-hand side to the target, and a flush lamp with an exposure time of 1 μs was synchronized to obtain a picture of the maximum bubble size. The plasma induced by the laser ablation was observed on the central axis of the target and the shadow of a hemispherical bubble, which was the laser cavitation, was observed using a lamp was placed on the other side of the camera.

Ultrasonic vibration is a popular method for generating cavitation for cleaning and/or sonochemistry. It is a well-known method for material testing of cavitation erosion resistance, which was standardized by ASTM International as ASTM G32, 16 (2016). Note that a standard test method for the erosion of solid materials by a cavitating liquid jet was also standardized by ASTM International (ASTM, G134, 17, 2017). Cavitation produced by ultrasonic vibration is called ultrasonic cavitation or acoustic cavitation, whereas cavitation that occurs in a flow field is called hydrodynamic cavitation. Fig. 3 shows a typical appearance of cavitation at the tip of the ultrasonic vibration horn. In Fig. 3, the tip of the horn was placed in water, and ultrasonic cavitation at the tip was observed from the bottom through a clear glass chamber. Cloud cavitation consisting of small tiny bubbles is illustrated in Fig. 3. Yamaguchi et al. (2002) proposed a micro-machining process applying ultrasonic cavitation. Rawers et al. (1991) found that ultrasonic cavitation introduced compressive residual stress into stainless steel powders, and Nakagawa and Watanabe (2004) demonstrated the introduction of compressive residual stress into the surface of bulk stainless steel. Gao et al. (2014) reported the ultrasonic cavitation peening of stainless steel and nickel alloys. Sasaki et al. (2016) investigated the effect of horn tip geometry on ultrasonic cavitation peening. Tan and Yeo (2017) proposed a surface smoothing method for AM components by ultrasonic cavitation with addition of an abrasive element. Kikuchi et al. (1991) reported that the intensity of ultrasonic cavitation drastically changed with the distance between the tip and the target, and Bai et al. (2018a) reported that a 0.2 mm increase in the distance reduced the processing capacity to 1/4. Therefore, careful geometry consideration is required when applying ultrasonic cavitation peening.

There are two mechanisms of impact involved in cavitation bubble collapse (Brennen, 1995). One is a microjet that is formed in a cavitation bubble, and the other is a shock wave due to rebound. As the speed of sound is approximately 1500 m/s in water, the strain speed caused by the microjet and/or shock wave is much higher than that of conventional shot peening. Therefore, the material properties of the

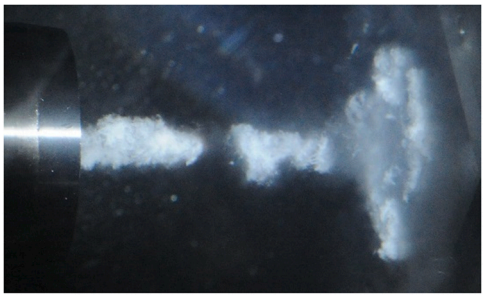

Fig. 1. Aspect of cavitation induced by a high-speed submerged water jet, i.e., a cavitating jet (Soyama, 2017).

Fig. 2. Aspect of laser ablation and laser cavitation induced by a pulsed laser, using double exposure photography (Soyama, 2020a).

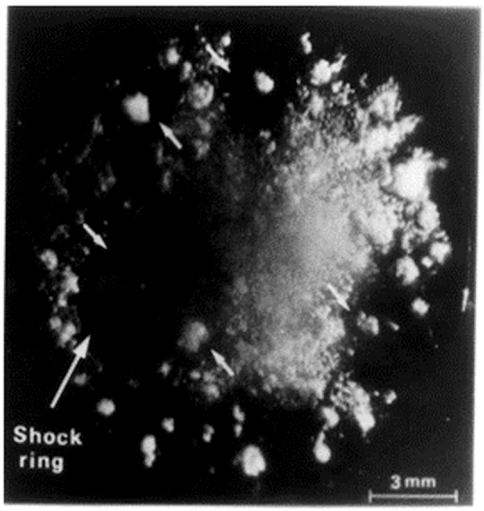

Fig. 3. Typical appearance of cavitation on tip of ultrasonic vibratory horn (Kikuchi et al., 1991).

surface-modified layer by cavitation peening have unique properties compared to those of conventional shot peening. For example, Soyama and Yamada (2008) found that cavitation peening introduced compressive residual stress, i.e., plastic strain, into quenched tool steel alloy while relieving micro strain. It was reported that cavitation peening modified deeper regions compared to shot peening at equivalent surface roughness. Therefore, it is worthwhile to review the material properties treated by cavitation peening in comparison with shot peening.

The advantages of cavitation peening are as follows. (1) The associated increase in surface roughness of relatively soft metals is more moderate than that of conventional shot peening, as shots are not used (Soyama et al., 2003). (2) As cavitation erosion starts after the incubation period when there is no mass loss (Thiruvengadam and Preseir, 1964), and cavitation peening is completed within approximately 1/100–1/5 of the incubation period, there is no damage with mass loss to the surface. (3) When the cavitating jet and ultrasonic vibration is used for cavitation peening, the thermal effect on the material surface is negligible. (4) Cavitation peening using the cavitating jet can treat complex shaped surface such as CVT element where the shot cannot directly reach (Soyama et al., 2008). Han et al. (2007) demonstrated that a surface parallel to the cavitating jet axis can be treated. The inner surface of the pipe whose diameter is smaller than the diameter of the cavitating region of the cavitating jet can also be treated by injecting a cavitating jet into the pipe. (5) Whilst the intensity of the cavitating jet is affected by hydraulic parameters such as upstream pressure p_1 and downstream pressure p_2 of the nozzle (Soyama, 2017), that of laser cavitation depends on the laser power (Soyama, 2021a), and that of the ultrasonic cavitation is changed by the amplitude of vibration (Gao et al., 2014). Thus, the peening intensity of cavitation peening can be controlled using these parameters. (6) Even though a high-speed water jet in air can treat a material surface (Daniewicz and Cummings, 1999), the working pressure of the cavitating jet is higher than that of the pump pressure for the injecting the water jet, as cavitation impact is utilized. (7) The treatment area of the cavitating jet at optimized condition is much wider than that of the water jet in air. (8) The range of optimal standoff distance, where the work sample is placed, of the cavitating jet is wider than that of the water jet in the air.

As cavitation is a hydrodynamic phenomenon and mechanical surface modification is material processing, the knowledge of both fluid dynamics and materials science is required. Therefore, in the present review, the mechanisms of cavitation peening using a cavitating jet, pulsed laser and ultrasonic vibration are explained, and the effects of cavitation peening are summarized in comparison with conventional shot peening, as shot peening is most popular peening method. Because dozens of papers were published recently. The direction of future work such as the required measurement parameters of materials properties for future experiments of cavitation peening is discussed based on the reported studies. As shown in Figs. 1 and 3, the bubble involved in aggressive cavitation is not spherical, and the importance of vortex cavitation and/or cloud cavitation for cavitation peening is also discussed.

2. Cavitation

Cavitation is a hydrodynamic phenomenon that involved phase change from the liquid phase to the gas phase due to an increase in fluid velocity (Brennen, 1995). Wang et al. (2021b) reported that the cavitation erosion caused by a vibratory horn was reduced by laser peening. Fig. 4 shows a schematic diagram of the development and collapse of bubbles during cavitation. Cavitation is initiated from the cavitation nuclei, tiny bubble(s) in water. Plesset and Chapman (1971) revealed the microjet at the collapse of a spherical bubble by numerical simulation, and Crum (1979) experimentally observed the microjet. Philipp and Lauterborn (1998) observed a shock wave at a bubble collapse. The microjet and shock wave are mechanisms by which cavitation produces plastic deformation and erosion of metallic materials.

When cavitation, which produced severe cavitation erosion, was observed, a cloud cavitation, which consisted from numerous tiny cavitation bubbles, was observed. As cloud cavitation was initiated from cavitation nuclei, it became cavitation in the vortex core, and then collapsed (see Fig. 4(b)). Thus, it is called vortex cavitation in the present review. Fig. 5 shows a typical aspect of vortex cavitation that was observed in the erosive area downstream from a butterfly valve (Soyama et al., 1994). Dominguez Cortazar et al. (1997) observed a microjet in vortex cavitation by using a special device called "Cavermod" (abbreviation of CAVitation ERosion MODel). In the case of a cavitating hydrofoil, severe erosive vortex cavitation was observed. As Tiwari (2015) reviewed, cavitation induced by ultrasonic has been utilizing the cleaning and chemical process. A wastewater treatment using cavitation induced by ultrasonic was also proposed Holkar et al. (2016). Gogate and Kabadi (2009) also reviewed about applications of ultrasonic and hydrodynamic cavitation in biochemical engineering. Cavitation bubble induced by a pulsed laser can be effective for cleaning in root canal Blanken et al. (2009).

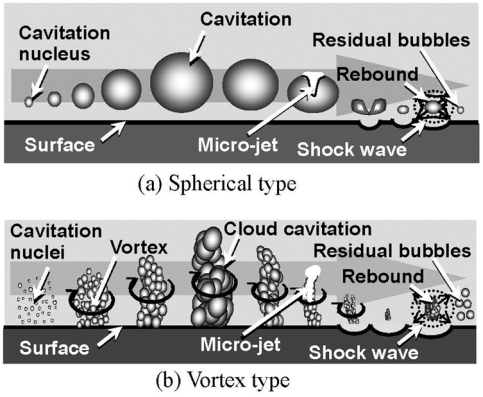

Fig. 4. Schematic diagram of development and collapse of cavitation (Soyama, 2017).

Fig. 5. Typical aspect of vortex cavitation, which produces severe impact (Soyama et al., 1994).

3. Cavitation peening

3.1. Cavitation peening using a water jet

3.1.1. Submerged high-speed water jet with cavitation (cavitating jet)

As aggressive cavitation is vortex cavitation, as mentioned above, vortex cavitation is generated by injecting a high-speed water jet into water, i.e., a cavitating jet. Fig. 6 shows the typical aspect of an impinging cavitating jet by observing a high-speed video camera (Soyama, 2020b), and Fig. 7 shows the peening area using pure aluminum. Fig. 8 illustrates a schematic of an impinging cavitating jet based on the observation of high-speed photography. In Fig. 6, the white bubbles are cavitation bubbles, as the camera and light are placed on the same side. Cavitation was initiated in the nozzle and/or in the shear layer at the nozzle exit. String-like vortex cavitation was observed as ring or helical vortex cavitation. Although pressurized water was continuously injected through a nozzle, cavitation clouds were periodically shed from the nozzle. It was reported that the cavitation cloud

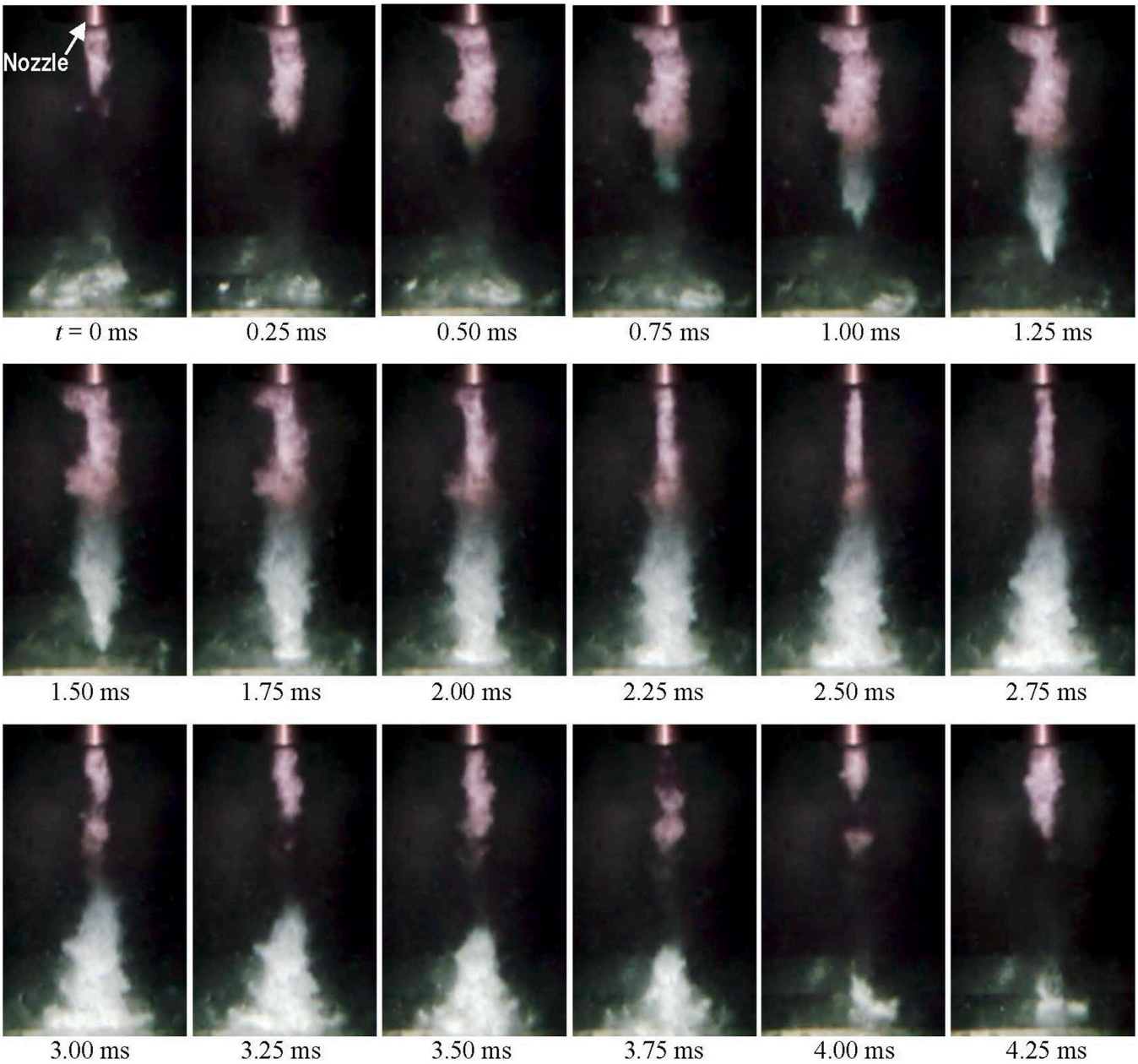

Fig. 6. Typical aspect of a cavitating jet in water (Soyama, 2020b).

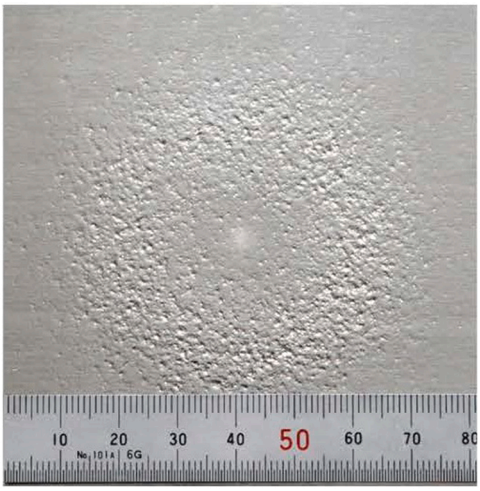

Fig. 7. Typical area peened by a cavitating jet, (Pure aluminum, $d = 2$ mm, $p_1 = 30$ MPa, $p_2 = 0.1$ MPa, $s = 262$ mm, $t = 1$ min) (Soyama, 2017).

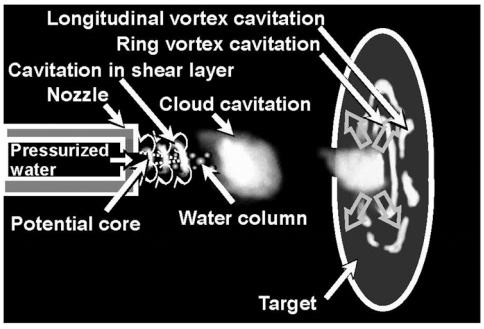

Fig. 8. Schematic diagram of an impinging cavitating jet.

shedding was governed by the phenomenon of the constant Strouhal number, which was defined by the shedding frequency, the width of the cavitating region, and the jet speed. When the cloud reached the impinging surface, it became a ring vortex cavitation, which is shown in Fig. 1 and Fig. 6 at $t = 1.75 – 3.25$ ms. Lastly, a part of vortex cavitation was collapsed after swelling like a crown. As impacts were produced at the collapse of the vortex cavitation, the peening area by the cavitating jet was a ring, as shown in Fig. 7. Then, at $t = 3.50$ ms, the next cavitation cloud was observed near the nozzle and the aspect is similar to that at $t = 0$ ms. Thus, the cloud shedding frequency was about 300 Hz.

3.1.2. Comparison between Water Jet Peening and Cavitation Peening Using a Water Jet

To distinguish between water jet peening and cavitation peening, Fig. 9 shows the weight loss of aluminum as a function of the standoff distance resulting from the impinging cavitating jet (Momma and Lichtarowicz, 1995). In Fig. 9, the cavitation number σ is defined by p_1, p_2, and the vapor pressure of water p_v as follows. As $p_1 >> p_2 >> p_v$ for the cavitating jet, σ is simplified as Eq. (1).

$$\sigma = \frac{p_2 - p_v}{p_1 - p_2} \approx \frac{p_2}{p_1} \tag{1}$$

In Fig. 9, two peaks were detected for each condition. In the present paper, the peak near the nozzle is named 1st peak, and the peak far from the nozzle is named 2nd peak. It was reported that 1st peak was suitable for cutting and 2nd peak was suitable for peening, as the process area at the 1st peak was small and that of 2nd peak was wide. The 1st peak was caused by the impinging impacts of the water column in the jet center, and the 2nd peak resulted from cavitation impacts. As lower σ

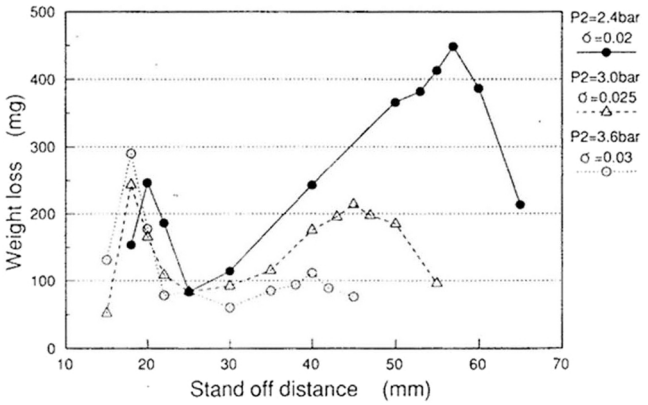

Fig. 9. 1st and 2nd peaks resulting from the cavitating jet at constant injection pressure for various cavitation number, (Momma and Lichtarowicz, 1995).

corresponded to the development of the cavitating region of the cavitating jet, the optimum standoff of the 2nd peak at lower σ was further, as shown in Fig. 9. As mentioned in the introduction, a peening method using the impinging impact of a water column is called water jet peening, and a peening method using cavitation impacts is called cavitation peening. Enomoto et al. (1996) reported the introduction of compressive residual stress into stainless steel by water jet peening using the submerged water jet, and Soyama et al. (1996a) revealed the introduction of compressive residual stress into stainless steel by cavitation peening using the cavitating jet.

To compare the peening intensity of water jet peening and cavitation peening, Kamisaka and Soyama (2018) investigated the peening intensity of water jet peening and cavitation peening by measuring the arc height of the plate specimen at various p_1. Fig. 10 shows the processing capability β at each optimum standoff distance of 1st peak (water jet peening) and 2nd peak (cavitation peening) changing with p_1 at constant p_2 (Kamisaka and Soyama, 2018). The β of water jet peening increased with p_1, as the working force of the water jet peening impinged the impact of the water column at the jet center. In contrast, β of cavitation peening had a maximum at $p_1 = 40$ MPa; it was 1.73 times larger than that of water jet peening at $p_1 = 60$ MPa. The jet power P_{jet}, which is the electricity power of the motor of the plunger pump, was defined by the flow rate Q and p_1, as shown in Eq. (2), P_{jet} at $p_1 = 40$ MPa was 54% of P_{jet} at $p_1 = 60$ MPa. The efficiency of cavitation peening was 3.2 times better than that of water jet peening.

$$P_{jet} = p_1 \quad Q \tag{2}$$

As it was suggested that the 1st peak was suitable for cutting and the 2nd peak was suitable for peening, water jet peening had a risk of damaging the surface. For example, Han et al. (2007) demonstrated an improvement in the fatigue strength of carbon steel 1045 by cavitation peening; however, Azhari et al. (2014) reported that water jet peening caused damage to the surface of carbon steel 1045. Therefore, it is worthwhile to distinguish which peening was used in the application. Thus, Soyama (2015) proposed a classification map by using the cavitation number σ and standoff distance s_{opt} normalized by the nozzle throat diameter d, as shown in Fig. 11. In Fig. 11, over 150 data points from the references are plotted. The 1st peak region, i.e., water jet peening and the 2nd peak region, can be classified by the line described by Eq. (3).

$$\frac{s_{opt}}{d} = 1.8 \quad \sigma^{-0.6} \tag{3}$$

The upper region of the line corresponds to the 2nd peak region, i.e., cavitation peening, and the lower region of the line corresponds to the 1st peak region, i.e., water jet peening.

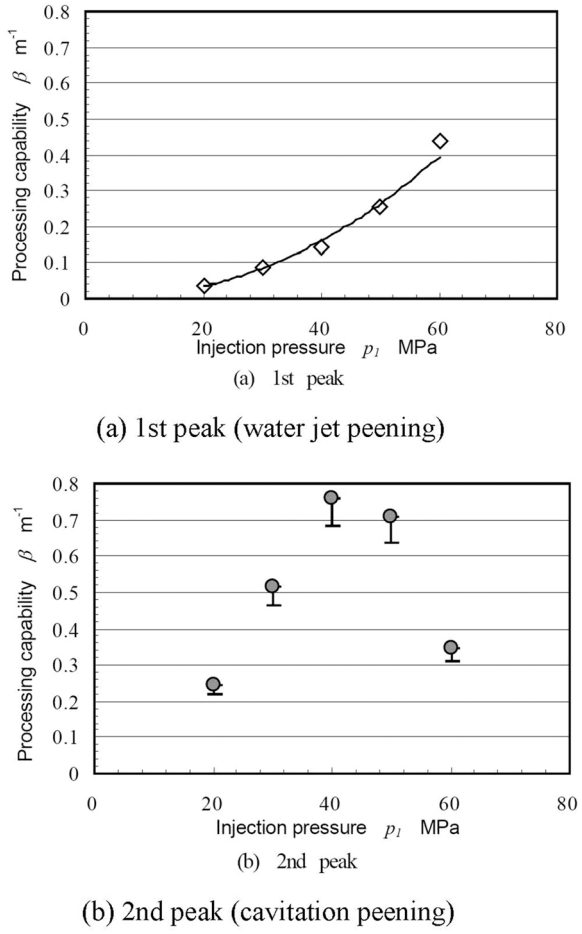

Fig. 10. Processing capability of a cavitating jet changing with injection pressure p_1 at constant downstream pressure, p_2 (Kamisaka and Soyama, 2018).

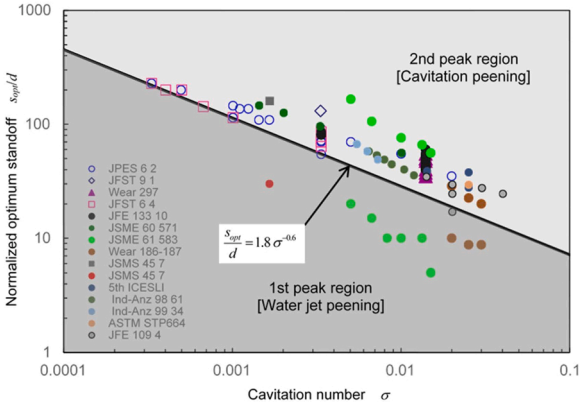

Fig. 11. Classification map for cavitation peening and water jet peening, considering the optimum standoff distance s_{opt}, where the aggressive intensity of the jet has a maximum, as a function of cavitation number σ (Soyama, 2015), (JPES 6 2: Soyama et al., 2012a; JFST 9 1:Soyama, 2014b; Wear 297: Soyama, 2013; JFST 6 4: Soyama and Takakuwa, 2011; JFE 133 10: Soyama, 2011; JSME 60 571: Yamauchi et al., 1994; JSME 61 583:Yamauchi et al., 1995; Wear 186–187: Momma and Lichtarowicz, 1995; JSMS 45 7: Hirano et al., 1996; JSMS 45 7: Enomoto et al., 1996; 5th ICESLI: Lichtarowicz and Scott, 1979; Ind-Anz 98 61: Kleinbreuer, 1976; Ind-Anz 99 34: Kleinbreuer, 1977; ASTM STP664: Lichtarowicz, 1979; JFE 109 4: Yamaguchi and Shimizu, 1987).

3.1.3. Cavitating jet in water and air

As mentioned above, the conventional cavitating jet was obtained by injecting the high-speed water jet into water, and it is named as "cavitating jet in water" in the present review. Mechanical surface modification by using "cavitating jet in air" was named by Soyama (2004). Marcon et al. (2016) conducted research on cavitating jet in air. Fig. 12 shows the typical aspect of a cavitating jet in water and air (Soyama, 2020b). In the case of a cavitating jet in air, a high-speed water jet was injected into a low-speed water jet, which was injected into water using a concentric nozzle. As the frequency of the cloud shedding and the wavy pattern of the low-speed water jet was synchronized at the optimum condition, the wavy pattern of the low-speed water jet was clearly observed at the optimum condition.

The cavitating jet in air can also treat targets such as the outside surface of pipes and tanks, but it has properties different than those of the cavitating jet in water. Fig. 13 illustrates the distribution of the residual stress of stainless steel SUS316L specimens treated by a cavitating jet in water and air, compared with non-peened specimens (Soyama, 2014a). Shimizu et al. (1997) reported that the mass loss caused by the cavitating jet with $p_1 = 98$ MPa had a peak at $\sigma = 0.01$–0.014, and it was also revealed that the mass loss of the cavitating jet with $p_1 = 20$ MPa had a peak at $\sigma = 0.014$. Namely, the aggressive intensity of the cavitating jet had a maximum at $\sigma \approx 0.014$. Thus, the residual stress distribution of the specimen treated by the cavitating jet at $\sigma = 0.014$ using a pressurized chamber was shown in Fig. 13. As shown in Fig. 13, the cavitating jet in air can introduce a large compressive residual stress in the subsurface region, where the compressive residual stress layer is relatively shallow. In comparison, the cavitating jet in water can introduce compressive stress in a relatively deeper region, and the compressive value at the surface is relatively smaller than that of the cavitating jet in air. The reason for this tendency is that pits introduced by the cavitating jet in air are dense and small, and the pits of the cavitating jet in water are coarse and large (Soyama, 2017). Cavitation peening using a cavitating jet in air corresponds to shot peening using a small shot at high velocity, and the cavitation peening using the cavitating jet in water corresponds to shot peening using a large shot at a relatively low velocity. Ogawa (2014) applied a cavitating jet in air for a skin-pass mill work roll. In the case of cavitation peening using a pressurized chamber, a large compressive stress was introduced into the subsurface and deeper regions.

3.2. Cavitation peening using a pulsed laser

3.2.1. Submerged laser peening and water-film laser peening

To explain the cavitation peening using a pulsed laser, Fig. 14 shows a schematic of laser peening and aspects of laser peening for (a) submerged laser peening and (b) water-film laser peening (Soyama, 2020c). The target was placed in a water-filled chamber for (a) submerged laser peening, and water was flowed like a film on the surface of a target for (b) water-film laser peening. In the case of the water-film laser peening, whose common name is "laser shock peening" (Clauer, 2019), the water film is flushed immediately after laser ablation, as shown in Fig. 15 (b). In the case of (a) submerged laser peening, a bubble was generated just after laser ablation, which developed, shrunk, and developed again, as shown in Fig. 15 (a). In the case of submerged laser peening, the bubble, which behaves like a cavitation bubble, is initiated after laser ablation. In the present review, the bubble after laser ablation is referred to as laser cavitation. The bubble collapse impact of laser cavitation can be utilized for peening. It was proposed cavitation peening using a pulsed laser to irradiate the focus in water near the target without ablation of the target. Gu et al. (2021b) investigated the effect of the distance between the focus point and the target surface.

In the case of water-film laser peening, Lu et al. (2017) investigated microstructural response and grain refinement mechanism of commercially pure titanium, Prabhakaran et al. (2019) show the effect of laser peening on microstructure and mechanical property of ultrafine bainitic

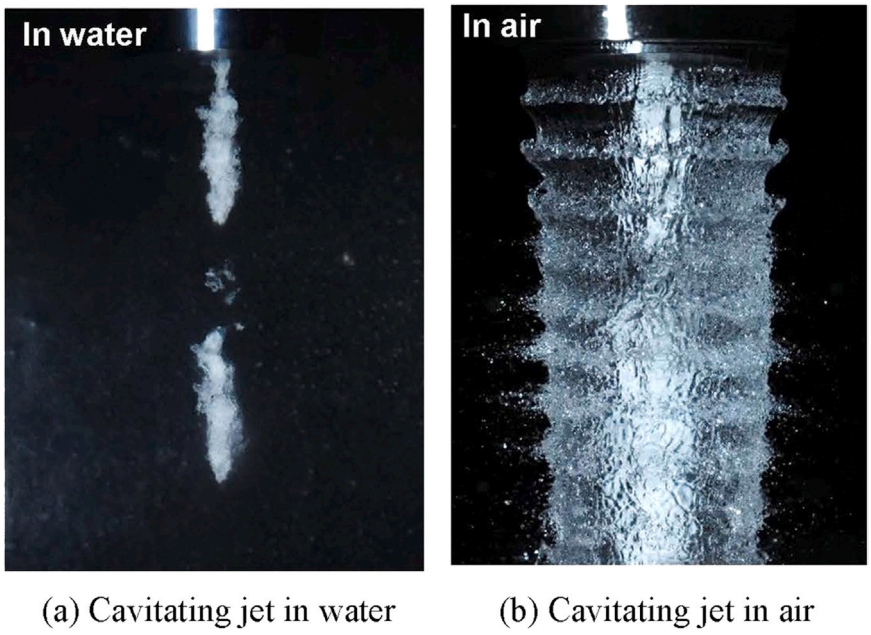

Fig. 12. Typical aspects of cavitating jet (Soyama, 2020b).

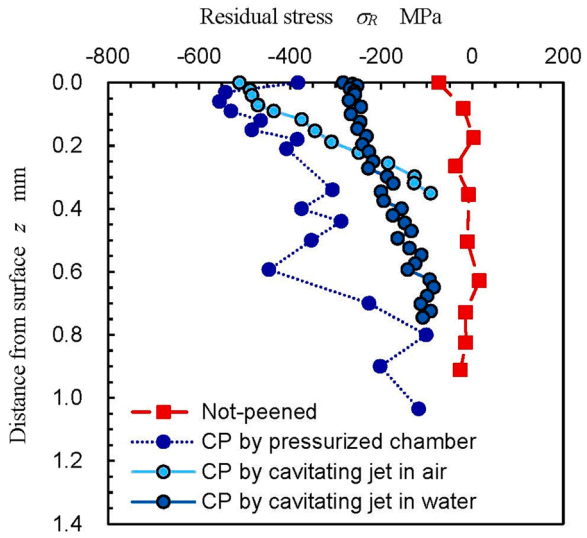

Fig. 13. Residual stress distribution with depth of stainless steel treated by various type of cavitating jet, (Soyama, 2014a).

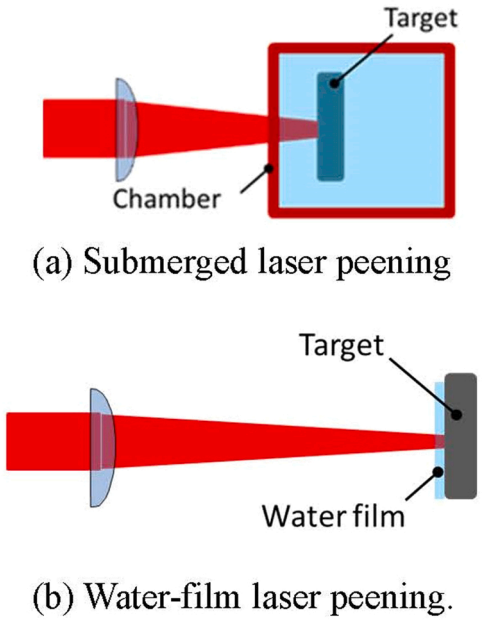

Fig. 14. Schematic diagram of laser peening (Soyama, 2020c).

steel, Lu et al. (2020) revealed the improvement in mechanical properties of additive manufactured titanium alloy, Sanchez et al. (2021) reported the effects of laser peening on the mechanisms of fatigue short crack initiation and propagation of aluminum alloy, Shukla et al. (2021) investigated the response of silicon nitride ceramics subject to laser peening, Wang et al. (2022) demonstrated the severe plastic deformation by observing nano-crystallization of martensitic laths and carbide deformation in stainless steel. Kaufman et al. (2022) investigated the effect of protective coating on intergranular corrosion of sensitized aluminum alloy using both submerged laser peening and water-film laser peening.

3.2.2. *Laser ablation and laser cavitation*

To investigate the impact intensity of laser ablation and laser cavitation, Fig. 16 shows (a) the aspect of laser ablation and laser cavitation, (b) signal from a PVDF sensor that was installed in the target, and (c) signal from the submerged shockwave sensor, which detects the amplitude of the shock wave in water (Soyama, 2021a). The impacts were detected at laser ablation ($t = 0$ ms) and at the collapse of laser cavitation ($t = 1$ ms) by the PVDF sensor, which detected the impact passing through the target material, and the impact of laser cavitation was larger than that of laser ablation. Note that the PVDF sensor was developed to evaluate the cavitation impact energy and improved by Soyama to protect the sensor surface. As shown in Fig. 16 (b), the impact induced by laser cavitation is larger than that of laser ablation. In contrast, when the shock wave in water was measured (see Fig. 16 (c)), the amplitude of the laser ablation was larger than that of laser cavitation, as Sasoh et al. (2005) reported. Takata et al. (2016) revealed that the amplitude of laser cavitation was larger than that of laser ablation under certain conditions when the amplitude of the signal from the AE sensor was measured. Note that the impact passing through the material

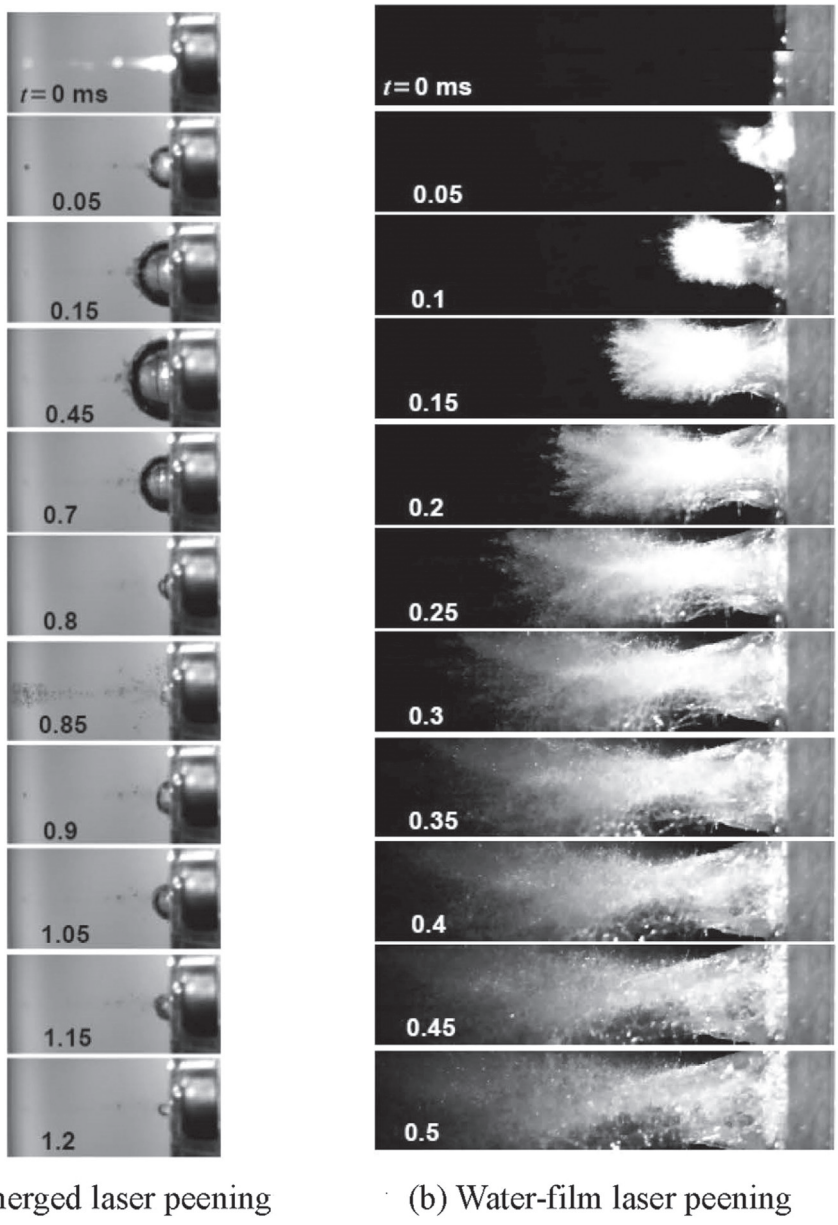

Fig. 15. Aspect of laser peening (Soyama, 2020c).

is more important than the shock wave in water, as peening is a material process.

To show the effect on materials of cavitation peening using a pulsed laser, Fig. 17 shows the residual stress and micro hardness changing with standoff distance; γ which is the distance between the focus point of the laser and the surface of the specimen for laser cavitation peening with coverage (LCP) and laser cavitation peening without coverage (LCPwc) investigated by Gu et al. (2021b). In the case of LCP, the compressive residual stress and micro hardness monotonously decrease with γ. In the case of LCPwc, the compressive residual stress and micro hardness ceased with γ, then decreased as laser ablation damaged the surface. Regardless, both LCP and LCPwc introduced compressive residual stress and work hardening.

3.3. Cavitation peening using ultrasonic

Ultrasonic cavitation induced by a vibratory horn, which is typically vibrating at 20 kHz, has been used for testing the cavitation erosion resistance (ASTM G32, 16, 2016) of materials. Takahashi et al. (1987) proposed a surface treatment of mild steel by ultrasonic cavitation and demonstrated the improvement of fatigue strength by the treatment. Rawers et al. (1991) revealed that ultrasonic cavitation could introduce compressive residual stress into stainless steel powders, and Nakagawa and Watanabe (2004) demonstrated that ultrasonic cavitation could introduce compressive residual stress into metallic plates such as pure Cu, Cu-Zn brass, and stainless-steel SUS304. Note that cavitation peening using ultrasonic means a peening method using cavitation impacts produced by ultrasonic vibration. On the other hand, in ultrasonic shot peening, collision impacts of shots which are accelerated by ultrasonic vibration are used (Abramov et al., 1998), and surface modifications such as nanocrystallization of the surface of 316 L stainless steel (Liu et al., 2000) and improvement of fatigue strength of welded part (Cheng et al., 2003) were reported.

Cavitation peening using ultrasonic with abrasive was also proposed; Kienzler et al. (2008) added abrasive grains in water and used the collision impact force of the abrasive grains to introduce compressive residual stress into low-alloyed tool steel. Tan and Yeo (2017) proposed the surface finishing of AM Inconel 625 to produce a smoother surface.

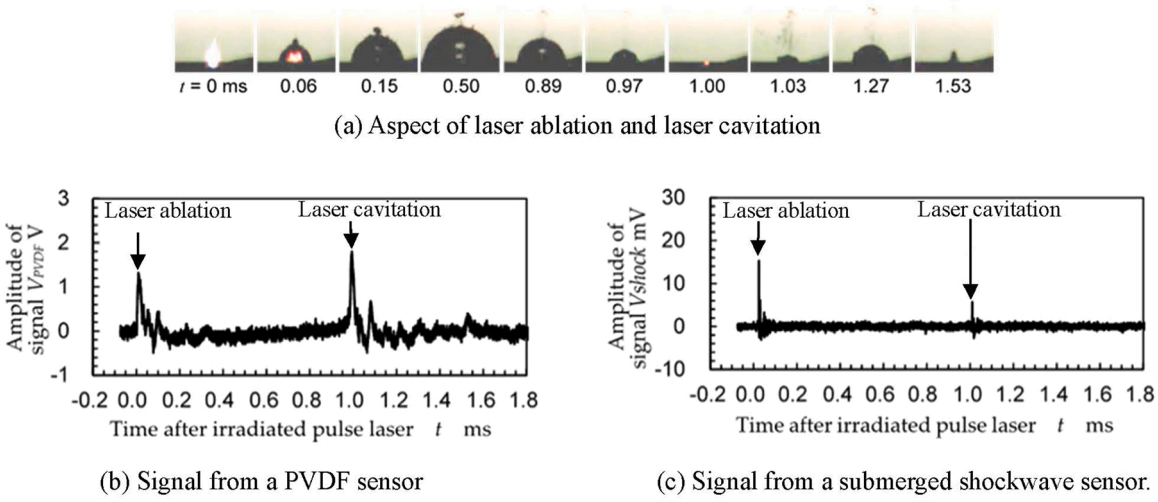

Fig. 16. Laser ablation and laser cavitation produced by a pulsed laser (Soyama, 2021a).

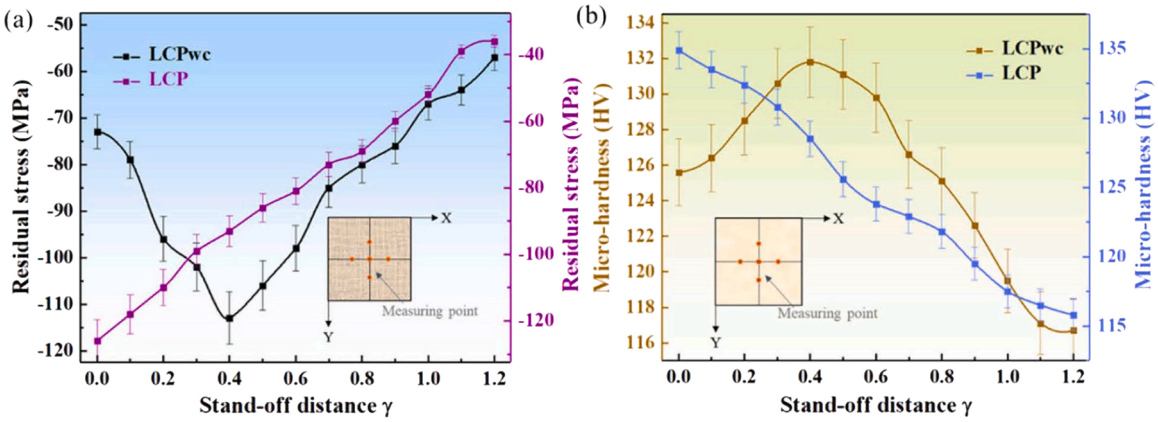

Fig. 17. Introduction of compressive residual stress and work hardening by laser cavitation peening LCP, i.e., cavitation peening using pulsed laser (Gu et al., 2021b).

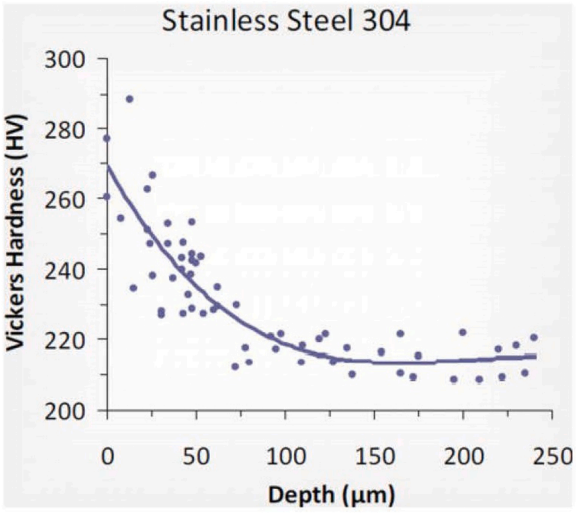

Fig. 18. Vickers hardness at different depths below the surface of stainless steel (Gao et al., 2014).

To show the effect of cavitation peening using ultrasonic waves, Fig. 18 shows the Vickers hardness as a function of the distance from the surface (Gao et al., 2014). In Fig. 18, the material was stainless steel 304, the used frequency was 20 kHz, the horn vibration amplitude was 20 μm, the distance between the specimen and the horn was approximately 1 mm, and the processing time was 10 min. As shown in Fig. 18, ultrasonic cavitation peening can introduce work hardening into the stainless steel surface.

The peening effect of ultrasonic cavitation, i.e., the aggressive intensity of ultrasonic cavitation, is affected by parameters such as the standoff distance between the horn and specimen and the horn vibration amplitude. Fig. 19 shows the volume change due to erosion by ultrasonic cavitation as a function of the standoff distance between the horn and the specimen for different amplitudes A at 40 μm and 45 μm. In Fig. 19, a large volume change corresponds to the large aggressive intensity of the ultrasonic cavitation. As shown in Fig. 19, the aggressive intensity had a peak at 0.5 – 0.8 mm of the standoff distance for both A = 40 μm and 45 μm. However, it was reduced to approximately 20% from 0.8 mm to 1.0 mm. Namely, the aggressive intensity of the ultrasonic cavitation using a vibratory horn was drastically changed by the standoff distance between the horn and the specimen. Thus, this effect should be considered when applying cavitation peening using ultrasonic waves.

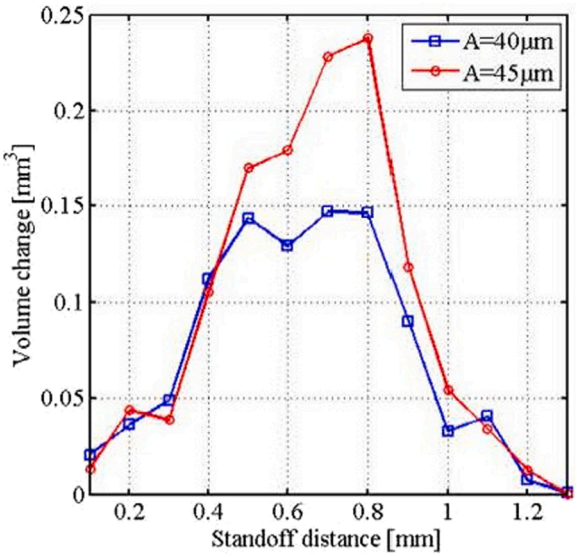

Fig. 19. Aggressive intensity of ultrasonic cavitation as a function of standoff distance between the specimen and the horn (Bai et al., 2018a).

4. Effects of cavitation peening comparing with shot peening

4.1. Fatigue strength

To reveal the comparison between cavitation peening and shot peening, Table 1 summarizes the fatigue strength of metallic materials of treated specimens by cavitation peening using a water jet (CP by jet), pulsed laser (CP by laser), and ultrasonic (CP by ultrasonic) compared with non-peened and shot peening (SP). In Table 1, the fatigue strengths are arranged in alphabetical order by the common names of materials, and the symbols in Table 1 are mainly following Japanese Industrial Standards JIS except SAE (Society of Automotive Engineers) 1045, as the most materials were following JIS. As shown in Fig. 13, the effect of cavitation peening using the jet strongly depends on the type of jet, i.e., the cavitating jet in water (CJW), the cavitating jet in air (CJA), and the cavitating jet in water using a pressurized chamber (CJW(P)). The injection pressure of jet p_1 is also a key parameter (Soyama, 2017). As the cavitating jet is the most popular cavitation peening, the type of jet and injection pressure are listed in Table 1. The types of fatigue tests, such as plane bending (PB), rotating bending (RB), and tension-tension (TT), were noted in the footnote at the end of Table 1. As the fatigue properties of the peened specimen strongly depend on that of the virgin material, i.e., the non-peened specimen, the results of the peened specimen including shot peening were summarized for the same number of specimens.

As mentioned above, Takahashi et al. (1987) demonstrated an improvement in the fatigue strength of mild steel by using ultrasonic CP. Soyama (2000) revealed the enhancement of the fatigue strength of silicon manganese steel using CP by a jet. Takahashi et al. (2018) reported that the fatigue strength of aluminum alloy A7075-T651 with a slit treated by the CJA was better than that of the shot-peened specimen (see Fig. 20). Soyama (2019) compared the fatigue properties of stainless-steel SUS316L treated by CP by jet, CP by laser, SP, and water jet peening at each optimum processing time, and found that the fatigue life of SP at 430 MPa was better than that of CP by jet. However, the fatigue strength of CP by jet was better than that of SP, as shown in Fig. 21. Soyama et al. (2021a) reported that the reduction in compressive residual stress introduced by CP by jet was smaller than that of SP; thus, the relief of introduced compressive residual stress would be one of the reasons.

To compare the improvement in fatigue strength between cavitation peening and SP, Fig. 22 shows the relation between the fatigue strength of the non-peened specimen σ_{fN} and the fatigue strength of peened specimen σ_{fP} for CP by jet, CP by laser, CP by ultrasonic, and SP by using data expressed in units of MPa in Table 1. Fig. 22 (a) shows the data for $0 < \sigma_{fN} < 850$ MPa, and Fig. 22 (b) shows the data for $0 < \sigma_{fN} < 400$ MPa. To quantitatively evaluate the improvement in fatigue strength by peening methods, Eq. (4) was assumed, and the improvement ratio k_f was obtained, and k_f is shown in Table 2.

$$\sigma_{fP} = k_f \quad \sigma_{fN} \tag{4}$$

The k_f in% is shown in Table 2 for $0 < \sigma_{fN} < 200$ MPa, $0 < \sigma_{fN} < 400$ MPa, and $0 < \sigma_{fN} < 850$ MPa. For example, in the case of CP by jet, the improvement ratio of the fatigue strength of metallic materials was $167 \pm 9\%$ for $0 < \sigma_{fN} < 200$ MPa, $147 \pm 6\%$ for $0 < \sigma_{fN} < 400$ MPa, and $121 \pm 9\%$ for $0 < \sigma_{fN} < 850$ MPa. The summarized data in Table 1 suggest that the improvement ratio was larger for relatively soft metallic materials for both cavitation peening and SP. The improvement ratio of CP by jet is nearly equivalent to and/or slightly better than that of SP. CP by laser and US can improve the fatigue strength, but the number of samples is not sufficient; therefore, more fatigue tests are required.

4.2. Work hardening and introduction of compressive residual stress

To show the peening effect on hardness and residual stress of cavitation peening compared with shot peening, Table 3 summarizes the Vickers hardness H_V and residual stress treated by cavitation peening CP using a jet, a laser, and ultrasonic compared with shot peening SP. In Table 3, the yield stress is included for reference, as Bregliozzi et al. (2005) reported effect of the yield stress on cavitation wear behavior and Chahine and Hsiao (2015) proposed a fluid–material interaction simulation of cavitation erosion considering the yield stress. As mentioned above, a cavitating jet is the most popular cavitation peening, and the type of jet and the injection pressure are indicated in Table 3, similar to Table 1. As shown in Table 3, the work hardening and introduction of compressive residual stress by cavitation peening have been reported for hard metals such as tool steel alloy SKD61, $H_V = 710$ (Sekine and Soyama, 2009), and soft metals such as aluminum alloy A5005, HV = 50 (Bai et al., 2018c).

To investigate work hardening by cavitation peening compared with shot peening, Fig. 23 shows the relation between the surface Vickers hardness of the non-peened $H_{V\,N}$ and that of the peened specimen $H_{V\,P}$. The hardening ratio k_{HV} was defined by Eq. (5), as presented in Table 4.

$$H_{VP} = k_{HV}\, H_{VN} \tag{5}$$

In Table 4, the correlation coefficient and the probability of non-correlation were calculated. As shown in Fig. 23 and Table 4, cavitation peening produces a work-hardening effect, and it is nearly the same order of SP. When the probability of a non-correlation is less than 1%, it can be concluded that the relationship is highly significant. In the case of SP and CP by jet and US, as the probability of non-correlation is less than 1%, it can be concluded that the relationships between the surface Vickers hardness of non-peened specimens and those of specimens peened by SP and CP by jet and US are highly significant. Namely, the harder metallic materials became harder due to work hardening by SP and CP by jet and US. In the case of CP using a laser without a protective layer, as the peened surface was ablated due to laser ablation, the work-hardening effect was not obvious in some cases. This is one of the reasons why the correlation coefficient was relatively small. As k_{HV} was 140% for SP and 128% for CP by jet, *the* k_{HV} of SP was larger than that of CP by jet. Kumagai et al. (2021) reported that the Vickers hardness of stainless steel treated by SP was larger than that of CP by jet and laser at equivalent arc-height conditions, and the dislocation density at the surface of SP was approximately 2.5 times that of CP by jet and laser. This suggests that a higher dislocation density of SP resulted in a higher hardness of SP. In all ways, CP can produce work hardening, and the

Table 1
Improvement of fatigue strength by cavitation peening by using a water jet, a pulsed laser and ultrasonic comparing with non-peened and shot peening.

Material	Fatigue test	Fatigue strength Non-peened	CP by jet	CP by laser	CP by US	SP	Type of jet	Injection pressure p_1 MPa	Reference
AM (EBM) titanium alloy Ti6Al4V	PB	169 MPa	296 MPa	317 MPa		335 MPa	CJW	30	Soyama and Okura (2018)
			280 MPa				CASF	60	Soyama and Sanders (2019)
			386 MPa				CASF+CJW	60 + 30	Sanders et al. (2021)
AM (DMLS) titanium alloy Ti6Al4V	PB	185 MPa	365 MPa	357 MPa		355 MPa	CJW	30	Soyama and Takeo (2020)
			280 MPa				CASF	60	Sanders et al. (2021)
			425 MPa				CASF+CJW	60 + 30	Sanders et al. (2021)
Aluminum alloy A2017	RB	120 MPa	185 MPa				CJW (P)	20	Soyama (2006)
Aluminum alloy A2017 with hole	TT	125 MPa	148 MPa			> 80 MPa	CJW	30	Takakuwa et al. (2016b)
Aluminum alloy A7075 without notch	PB	260 MPa	320 MPa			320 MPa	CJA	30	Takahashi et al. (2018)
Aluminum alloy A7075 with 0.1 mm notch	PB	140 MPa	280 MPa			320 MPa	CJA	30	
Aluminum alloy A7075 with 0.2 mm notch	PB	100 MPa	280 MPa			200 MPa	CJA	30	
Aluminum alloy AC4CH	RB	96 MPa	145 MPa				CJW (P)	30	Soyama et al. (2002)
Aluminum alloy AC4CH	RB	97 MPa	156 MPa			120 MPa	CJW (P)	30	Soyama et al. (2003)
Aluminum alloy AC4CH	RB	88 MPa	120 MPa				CJA	30	Soyama and Miyamoto (2015)
			120 MPa				CJW (P)	30	
Aluminum alloy AC8AH	RB	106 MPa	124 MPa				CJA	30	Soyama and Miyamoto (2015)
			140 MPa				CJW (P)	30	
Carbon steel SAE1045	TT	170 MPa	300 MPa				CJW	30	Han et al. (2007)
Carbon tool steel SK5 (CVT element)	PB	156 N	231 N				CJW (P)	30	Soyama et al. (2008)
Carburized chrome molybdenum steel SCM415	RB	733 MPa	832 MPa			785 MPa	CJW (P)	30	Odhiambo and Soyama (2003)
Carburized chrome molybdenum steel SCM415 (Gear)	PG	1900 MPa	2120 MPa				CJW	30	Seki et al. (2008)
Carburized chrome molybdenum steel SCM420	RB	777 MPa	931 MPa			915 MPa 918 MPa	CJW (P)	30	Soyama (2006)
Chrome molybdenum steel SCM420H (Gear)	PG	337 Nm	418 Nm			376 Nm	CJW (P)	30	Soyama and Sekine (2010)
Chrome molybdenum steel (Bolt)	DF	327 MPa	505 MPa				CJW (P)	30	Kumagai et al. (2016)
Chromium steel SCr420 (Roller)	RT	2070 MPa	2180 MPa			2270 MPa	CJW	30	Seki et al. (2012)
FSWed aluminum alloy AA5754	PB	121 MPa	156 MPa				CJA	20	Soyama et al. (2021c)
Induction hardened Carbon steel S50C	PB	525 MPa	700 MPa				CJA	30	Fukuda et al. (2008a)
Magnesium alloy AZ31B	PB	97 MPa	111 MPa	151 MPa		104 MPa	CJW	30	Soyama (2021b)
Magnesium alloy AM60B	RB	88 MPa	104 MPa				CJA	30	Soyama and Miyamoto (2015)
Mild steel	US	350 MPa			390 MPa		CP by US only		Takahashi et al. (1987)
	RB	190 MPa			200 MPa				
Nitrocarburized Steel S50C	PB	668 MPa	772 MPa				CJA	30	Fukuda et al. (2008b)
Nickel chrome molybdenum steel SNCM420 (Gear)	GB	849 MPa	937 MPa			910 MPa	CJW (P)	30	Soyama and Macodiyo (2005)
			903 MPa			915 MPa	CJW (P)	50	
Quenched carbon steel SAE1045	TT	200 MPa	350 MPa				CJW	30	Han et al. (2007)
Silicon manganese steel SUP7	4PB	400 MPa	440 MPa				CJW (P)	30	Soyama (2000)
Silicon manganese steel SUP7	RB	820 MPa	940 MPa				CJW (P)	30	Soyama et al. (2001)
Stainless-steel 316 L	PB	279 MPa	360 MPa				CJA	30	Soyama (2007)
			327 MPa				CJW	30	
Stainless-steel 316 L	RB	190 MPa	240 MPa			340 MPa	CJW (P)	30	Masaki et al. (2008)
Stainless-steel 316 L	PB	279 MPa	348 MPa	272 MPa		305 MPa	CJW	30	Soyama (2019)
Stainless-steel 316 L	PB	266 MPa	345 MPa			335 MPa	CJW	30	Soyama et al. (2021a)
Stainless-steel 316 L (welded)	PB	188 MPa	242 MPa	300 MPa		260 MPa	CJW	30	Soyama (2021a)
Titanium alloy Ti6Al4V	FF	315 MPa	390 MPa			400 MPa	CJW (P)	30	Lee et al. (2009)
Titanium alloy Ti6Al4V-ELI (Spinal implant)	FF	150 N	325 N				CJW (P)	80	Takakuwa et al. (2016a)

* 1 AM in "Material" means additive manufacturing.
* 2 CJW and CJA in "Type" mean cavitating jet in water and air. (P) means the use of pressurized chamber. CASF means cavitation abrasive surface finishing, i.e., cavitating jet in water with abrasive.
* 3 PB, 4PB, RB, TT, DF, FF, GB, PG, RT, US in "Fatigue test" mean plane bending, 4-point bending, rotating bending, tension-tension, delayed fracture, fretting fatigue, gear bending, power circulating-type gear test, roller testing, ultrasonic fatigue test.

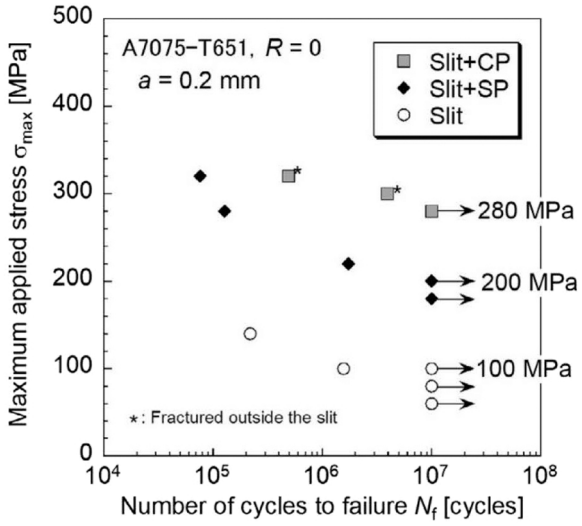

Fig. 20. Improvement of fatigue strength by cavitation peening using a cavitating jet in air comparing with shot peening (Takahashi et al., 2018).

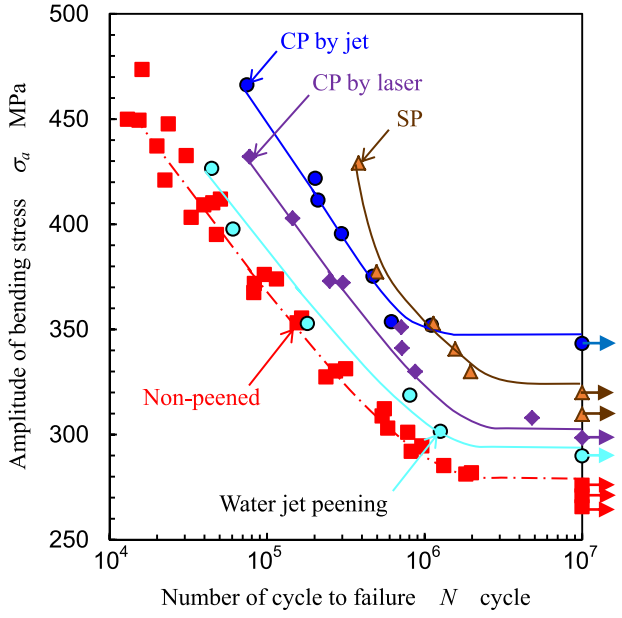

Fig. 21. Improvement in fatigue strength by the various peening methods (Soyama, 2019).

increase in hardness by CP is approximately 30%, which is smaller than that of SP. This would be a guide for the work hardening of CP.

As shown in Table 3, there are many reports on the introduction of compressive residual stress by cavitation peening. Vidvans et al. (2021) revealed the distribution of residual stress of aluminum alloy A7075-T651 introduced by the CJA compared with SP and laser peening, which is a water-film type (see Fig. 24). Takahashi et al. (2018) also reported the introduction of compressive residual stress into aluminum alloy A7075-T651 by a CJA and SP. Both methods show that the compressive residual stress on the surface introduced by cavitation peening was larger than that of SP. Takahashi et al. (2018) reported that the compressive residual stress introduced by the CJA had a maximum at the surface, as shown in Fig. 13; however, Marcon et al. (2018) and Vidvans et al. (2021) revealed that the surface compressive residual stress introduced by the cavitating jet was slightly lower than that of the subsurface layer.

With regard to the effect of processing time on the introduction of compressive residual stress, Mathias et al. (1991) revealed that the surface compressive residual stress of chrome molybdenum steel increased with exposure time to ultrasonic cavitation until erosion started. Sekine and Soyama (2009) reported that the longer processing time of the cavitating jet introduced larger compression into the tool steel alloy SKD61, and then the compressive residual stress was saturated at a certain processing time. Namely, cavitation peening has an optimum processing time for the introduction of compressive residual stress as well as other peening methods.

To compare the introduction of compressive residual stress at the optimum processing time between peening methods, Fig. 25 illustrates the residual stress σ_R of stainless steel SUS316L as a function of distance from the surface z for SP, water jet peening, CP by jet, and laser. The optimum processing time and density of the pulsed laser were defined by the fatigue life at $\sigma_a = 400$ MPa, which changed with the processing time and density of the pulsed laser. The residual stress was evaluated by the 2D method using X-ray diffraction (XRD), and the details of the measurement conditions are provided in Soyama et al. (2021c). In the case of CP by jet and water jet peening, the compressive residual stress had a maximum at the surface. It is well known that the compressive residual stress introduced by SP has a maximum at a certain depth. In the case of CP by laser ablation, the residual stress on the surface was nearly zero. Although CP by jet resulted in the largest fatigue strength (Soyama, 2019), the introduced compressive residual stress was not significant. Namely, cavitation peening introduces compressive residual stress into metallic materials, but a fatigue test is required to compare the fatigue strength, as the fatigue strength of the samples treated by different peening methods cannot be estimated by the residual stress distribution.

To investigate the key parameters of the mechanical properties of the materials, Fig. 26 shows the relation between the yield stress of the base metal and the introduced compressive residual stress, and Table 5 shows the correlation coefficient between them. For all peening methods, Fig. 26 shows that the larger the yield stress, the larger the compressive residual stress is. However, the correlation coefficients are not large.

Fig. 27 illustrates the relationship between the Vickers hardness of the non-peened surface and the introduced compressive residual stress, and Fig. 28 shows the relationship between the Vickers hardness of the peened surface and the introduced compressive residual stress. Table 6 shows the correlation coefficient between the Vickers hardness of the non-peened surface and the introduced compressive residual stress, and Table 7 shows the correlation coefficient between the Vickers hardness of the peened surface and the introduced compressive residual stress. The harder the metallic materials, the larger the introduced compressive residual is. When Figs. 26–28 were compared considering Tables 5–7, the introduced compressive residual stress had a better correlation with the Vickers hardness than the yield stress of bulk metals.

5. Numerical simulation of cavitation peening

5.1. Simulation of cavitation peening by using the jet

In the case of numerical simulation of shot peening, the boundary condition, i.e., solid-solid contact such as Hertzian contact is well

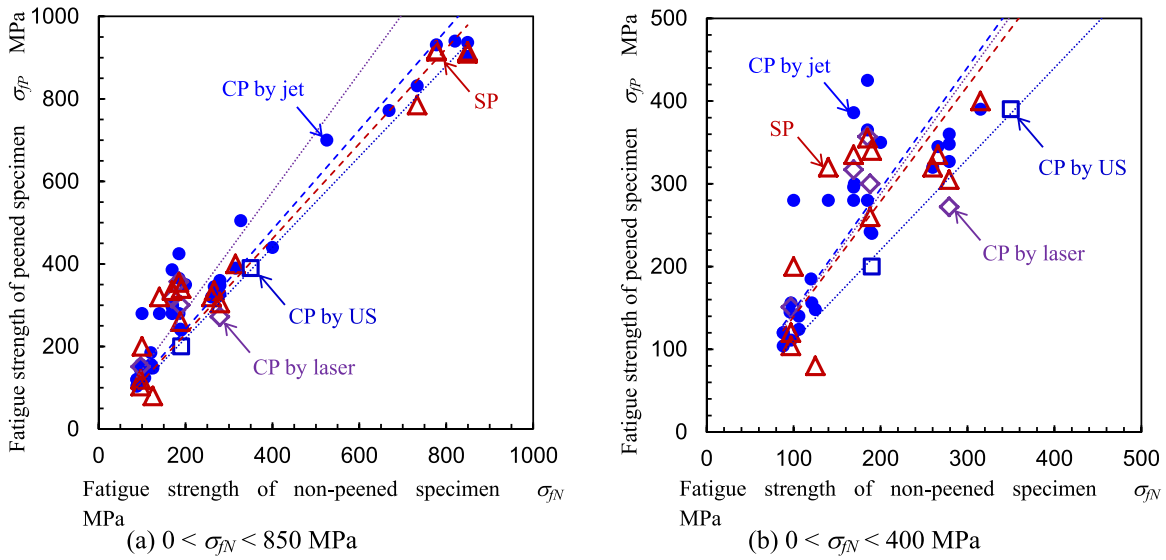

Fig. 22. Improvement of fatigue strength by cavitation peening comparing with shot peening.

Table 2
Improvement ratio of fatigue strength k_f by peening methods comparing with non-peened.

Range of σ_{fN}	CP by jet	CP by laser	CP by US	SP
$0 < \sigma_{fN}$ < 200 MPa	167 ± 9% [22]	177 ± 9% [4]	105% [1]	168 ± 16% [9]
$0 < \sigma_{fN}$ < 400 MPa	147 ± 6% [30]	144 ± 21% [5]	110 ± 3% [2]	139 ± 10% [13]
$0 < \sigma_{fN}$ < 850 MPa	121 ± 9% [38]	144 ± 21% [5]	110 ± 3% [2]	115 ± 4% [18]

* 1 Value in [] reveals the number of datasets in Table 1.

known, and applies stress distribution of the shot impact to the target surface can be assumed, then the numerical simulation can be conducted. On the other hand, currently, numerical simulation of cavitation impact is still a major problem in the estimation of cavitation erosion. Namely, the applied stress distribution at cavitation impact is unknown. Thus, in the case of numerical simulation of cavitation peening using the jet, i.e., hydrodynamic cavitation, both knowledge of fluid dynamics and elastoplastic of materials is required.

Han et al. (2010) reported the residual stresses of pure titanium treated by cavitation peening using a cavitating jet using the combined finite-element method (FEM) with the dislocation density method (DDM). Chahine et al. (2016) simulated cavitation peening and pitting by coupling bubble and material dynamics, and they revealed the residual stress distribution introduced by the collapse of a single bubble near a solid surface. As mentioned above, in the case of the cavitating jet, cloud cavitation consisted of many tiny bubbles, which became a vortex cavitation and then collapsed. Ma et al. (2018) simulated the cloud collapse, which is shown in Fig. 29, and reported that the bubble cloud produced higher pressure loading at the wall when the excitation pressure amplitude increased. These calculation results are consistent with the experimental results, which are that cavitation becomes more aggressive as the downstream pressure of the nozzle increases (Soyama, 2017).

Peng and Shimizu (2013) reviewed the progress of cavitation modeling and numerical simulation of cavitating water jets, and Peng et al. (2016) attempted to simulate cavitation cloud shedding in a submerged water jet by numerical analysis. Tan et al. (2018b) simulated the cavitating region of a cavitating jet and reported the effect of nozzle geometry on the cavitating region. Simulations were performed such that cavitation in the shear layer of the cavitating jet creates a ring-shaped peening area, as shown in Fig. 7 by Sonde et al. (2018) and Liu and Ma (2021). However, the ring-shaped peening area resulted from vortex cavitation in the impinging area, as shown in Figs. 6 and 8. Thus, the considerations of cloud cavitation and the vortex cavitation on the impinging surface are required for the simulation. Considering the pressure distribution on the impinging surface, which was reported by Soyama and Lichtarowicz (1996) and Nobel and Talmon (2012), the ring-shaped peening area can be explained by the potential flow, when the local cavitation number on the impinging surface is taken into consideration by Soyama (2020b).

As the impacts at bubble collapse are caused by microjet and shock wave at the rebound, the strain speed of the deformation is considerably higher than that of conventional shot peening. Gurrutxaga, Lerma et al. (2020) reviewed the mechanics and physics of high-speed dislocations, Ansari et al. (2020) carried out the numerical analysis of high-speed water jet spot welding using the arbitrary Lagrangian-Eulerian (ALE) method with Johnson-Cook model, Zhang et al. (2021) simulated the deformation of aluminum alloy treated by ultrasonic shot peen forming considering Johnson-Cook model. Thus, at the numerical simulation of cavitation peening, the strain rate should be considered.

5.2. *Simulation of cavitation peening by using the pulsed laser*

In the case of water-film laser peening, Peyre et al. (2003) carried out FEM simulation of residual stresses induced by laser peening and Zhang et al. (2004) simulated the effect of laser peening on the layered film structure by 3D stress/strain analysis, Keller et al. (2018) compared the residual stress by experimental and numerical investigation and so on. However, in the case of laser cavitation, i.e., submerged laser peening, few researches have been carried out, as most of researchers believes that submerged laser peening is using the ablation impact (Sano et al., 2020). On the other hand, in the research area of bubble dynamics, most of the researchers are interested in bubble near the boundaries as Blake and Gibson (1987) simulated the bubble near the boundaries, not on the solid surface. Then, in the case of laser cavitation for peening, Dabir--Moghaddam et al. (2017) simulated not only hemispherical bubbles but also pan-cake type bubbles. Gu et al. (2021b) reported the relationship between the position of the laser cavitation and the pressure induced by the bubble collapse. Gu et al. (2021a) simulated the equivalent plastic strain and residual stress caused by multiple laser cavitation impacts compared with the experimental results (see Fig. 30).

Table 3
Work hardening and introduction of compressive residual stress by cavitation peening by using a water jet, a pulsed laser ultrasonic comparing with non-peened and shot peening.

Material	Yield stress σ_y MPa	Vickers hardness					Residual stress σ_R MPa					Type of jet	Injection pressure p_1 MPa	Reference
		Non-peened	CP by jet	CP by laser	CP by US	SP	Non-peened	CP by jet	CP by laser	CP by US	SP			
AM (EBM) titanium alloy Ti6Al4V	196	344	367	338		386	-220	-648	-450		-348	CJW	30	Okura et al. (2020)
AM (SLM) stainless-steel 316 L		172			266									Wang et al. (2021a)
Aluminum alloy A2017	258	130	160	280		180	20	-297	-211		-248	CJW	30	Kokubun and Soyama (2017)
Aluminum alloy A2030-T3	250	160			184							CP by US only		Janka et al. (2016)
Aluminum alloy A5005		55			75							CP by US only		Bai et al. (2018b)
Aluminum alloy A5005		50			68							CP by US only		Bai et al. (2018c)
Aluminum alloy A5050		57			87							CP by US only		Bai et al. (2021)
Aluminum alloy A5754		75	77				0	-120				CJA	20	
Aluminum alloy A6061		70	82.5					-129				CJW	20	Yang et al. (2021)
Aluminum alloy A6063-T6	150	83	101				-20	-90				CJW	60	Grinspan and Gnanamoorthy (2007)
Aluminum alloy A7075-T651	[549]	[210]					25	-400			-325	CJA	34	Marcon et al. (2018)
Aluminum alloy A7075-T651	549	210	230			240		-380			-450	CJA	30	Takahashi et al. (2018)
Aluminum alloy A7075-T651	[549]	[210]					-60	-450			-350	CJA	34	Vidvans et al. (2021)
Aluminum alloy AC4CH	(245)	104					-126	-219				CJW (P)	30	Soyama et al. (2002)
Aluminum alloy AC4CH	(245)	104					-60	-160				CJW (P)	30	Soyama et al. (2003)
Aluminum alloy 2A02	280	135		142			-5		-52			CP by laser only		Ren et al. (2018)
Aluminum alloy 2A12							-60	-320				CJW	20	Tan et al. (2018a)
Aluminum alloy 2A70	310						-5		-97			CP by laser only		Zhang et al. (2019)
Aluminum copper alloy		121	148				23	-224				CJW	35	Ijiri et al. (2019)
Aluminum lithium alloy 8090Al–Li	90	160	199				-137	-162				CJW	30	Sekyi-Ansah et al. (2021)
Carbon steel Q235	235			135					-126			CP by laser only		Gu et al. (2021b)
Carbon steel AISI1045							-40			-200		CP by US only		Mathias et al. (1991)
Carbon steel SAE1045							70	-210				CJW	30	Han et al. (2007)
Carburized chrome molybdenum steel SCM415							240	-560				CJW (P)	30	Odhiambo and Soyama (2003)
Carburized chrome molybdenum steel SCM415 (Gear)		715	783				-385	-661				CJW	30	Seki et al. (2008)
Carburized chrome molybdenum steel SCM420		753					-50	-553			-1106 -1327	CJW (P)	30	Soyama (2006)
Chrome molybdenum steel SCM435							200	-250				CJW	35	Tanaka et al. (2019)
Chrome molybdenum steel AISI4140	800						-40			-380		CP by US only		Mathias et al. (1991)
Chrome molybdenum		430						-610 -650 -660			-600	CJA CJW	30 30 30	Klumpp et al. (2017)

(*continued on next page*)

Table 3 (*continued*)

Material	Yield stress σ_y MPa	Vickers hardness					Residual stress σ_R MPa					Type of jet	Injection pressure p_1 MPa	Reference
		Non-peened	CP by jet	CP by laser	CP by US	SP	Non-peened	CP by jet	CP by laser	CP by US	SP			
steel AISI4140												CJW (P)		
Chrome molybdenum steel (Bolt)							269	-178				CJW (P)	30	Kumagai et al. (2016)
Chromium steel SCr420 (Roller)		760	888			1170 975	-370	-724			-547 -1000	CJW	30	Seki et al. (2012)
Copper C1100		93					-60	-175				CJW (P)	20	Soyama et al. (2000)
Electrical steel sheet	372						-200	-450				CJW (P)	30	Takakuwa et al. (2011)
FSWed aluminum alloy AA5754		62	60				20	-50				CJA	20	Soyama et al. (2021b)
Gray cast iron HT200		215							-275			CP by laser only		Gu et al. (2020)
High-speed steel M2 HSS		698					-12	-823				CJW	27	Latchoumi et al. (2019)
Induction hardened carbon steel S50C		500					0	-750				CJA	30	Fukuda et al. (2008a)
Magnesium alloy AM60B							-40	-100				CJA	30	Sekine et al. (2008)
Molybdenum-based high-speed steel	549	698	1058				-12	-954				CJW	27	Balamurugan et al. (2018)
Nickel alloy 200	83	116			154							CP by US only		Gao et al. (2014)
Nickel-based alloy NCF600	367	173					400	-500				CJW	70	Saitou et al. (2003)
Nickel-based superalloy IN718 SPF	1070		315					-700 -800				CJA CJW (P)	30 30	Gill et al. (2013)
Nitrocarburized Steel S50C		377	413				-300	-400				CJA	30	Fukuda et al. (2008b)
Nickel chrome molybdenum steel SNCM420 (Gear)		716						-840 -750			-840 -1090	CJW (P) CJW (P)	30 50	Soyama and Macodiyo (2005)
Nickel chrome molybdenum steel SNCM630							40	-400				CJW	35	Tanaka et al. (2019)
Quenched carbon steel SAE1045							-250	-530				CJW	30	Han et al. (2007)
Silicon manganese steel SUP7	1225	397					-18	-419				CJW (P)	30	Soyama (2000)
Silicon manganese steel SUP7	1245	567					-470	-690				CJW (P)	30	Soyama et al. (2001)
Spring steel SAE1070		[471]					-350	-610				CJW	30	Qin et al. (2006)
Spring steel SAE1070		[471]						-650				CJW	32	Han et al. (2013)
Stainless mold steel		HRC35 HRC49					-20 0			-410 -620		CP by US only		Toh (2007)
Stainless-steel 304	235						180	-600 -550				CJW CJW	30 70	Soyama et al. (1996a)
Stainless-steel 304	275						200	-300				CJW	60	Hirano et al. (1996)
Stainless-steel 304							40			-594				Sriraman and Vasudevan (1998)
Stainless-steel 304							-50	-700				CJW (P)	20	Soyama et al. (2000)
Stainless-steel 304	355	180					400	-300				CJW	70	Saitou et al. (2003)
Stainless-steel 304								-480			-440	CJW	30	Turski et al. (2010)
Stainless-steel 304	196	230	362	354		371	-30	-377	-470		-519	CJW	30	Lesyk et al. (2019)
Stainless-steel 304	207–276	227			269							CP by US only		Gao et al. (2014)
Stainless-steel 304	350	260			547							CP by US only		Janka et al. (2016)
Stainless-steel 304	280									-300		CP by US only		Lim et al. (2021)
Stainless-steel 304			264									CJW	20	Yang et al. (2021)
Stainless-steel 316							0	-700				CJW (P)	20	Soyama et al. (2000)

(*continued on next page*)

Table 3 (*continued*)

Material	Yield stress σ_y MPa	Vickers hardness					Residual stress σ_R MPa					Type of jet	Injection pressure p_1 MPa	Reference
		Non-peened	CP by jet	CP by laser	CP by US	SP	Non-peened	CP by jet	CP by laser	CP by US	SP			
Stainless-steel 316 L	315	270	285				400	-350				CJW	70	Saitou et al. (2003)
Stainless-steel 316 L		160	200			300	-180	-500			-650	CJW (P)	30	Masaki et al. (2008)
Stainless-steel 316 L	[308]	180					41	-510				CJA	30	Soyama et al. (2011a)
Stainless-steel 316 L	[308]	180					41	-283				CJW	30	Soyama and Takakuwa (2011)
								-192				CJW	100	
								-229				CJW	150	
								-199				CJW	200	
								-224				CJW	250	
								-220				CJW	300	
Stainless-steel 316 L	[309]	[160]					-80	-500	-600		-600	CJA	30	Soyama (2014a)
								-550				CJW	30	
Stainless-steel 316 L	216	168	270	272		319	-11	-124	-65		-173	CJW	30	Soyama (2019)
Stainless-steel 316 L	304	175	244	240		245	10	-303	-175		-401	CJW	30	Soyama (2020d)
Stainless-steel 316 L	309	160	240			273	29	-184			-234	CJW	30	Soyama et al. (2021a)
Stainless-steel 316 L	[309]	[160]					[29]	-300	-640		-400	CJW	30	Soyama et al. (2021c)
Stainless-steel 316 L	308	200	350	350		370	12	-470	-530		-575	CJW	30	Kumagai et al. (2021)
Steel Plate Cold Commercial							0			-210		CP by US only		Jung et al. (2017)
Steel Plate Cold Commercial							0			-140		CP by US only		Jung et al. (2018)
Steel tube for heat transfer NCF600		180	222				0	-300				CJW (P)	120	Ohya et al. (2000)
Structural steel Q235		118		182			-9		-273			CP by Laser only		Gu et al. (2021a)
Titanium		152	167				-150	-620				CJW	30	Ju and Han (2009)
Titanium alloy TC4	821	330	441				-100	-846				CJW	40	He et al. (2021)
Titanium alloy TC4	821		341					-206				CJW	15	Li et al. (2021)
			357					-328					20	
			427					-729					30	
			416					-552					40	
Titanium alloy Ti6Al4V		335					-270	-950			-800	CJW (P)	30	Soyama et al. (2004)
Titanium alloy Ti6Al4V		335					-150	-1000				CJW (P)	30	Lee et al. (2009)
Titanium alloy Ti6Al4V-ELI (Spinal implant)		500	960				-116	-628				CJW (P)	80	Takakuwa et al. (2016a)
Tool steel alloy SKD61		[710]						-300	-900		-900	CJA	20	Soyama (2004)
									-800			CJW (P)	20	
Tool steel alloy SKD61		[710]						-600	-1000			CJA	30	Soyama and Yamada (2008)
Tool steel alloy SKD61		710	830					-560	-1210			CJW (P)	30	Sekine and Soyama (2009)
Tool steel alloy Toolox44		448					-20			-480				Kienzler et al. (2008)

* 1 AM in "Material" means additive manufacturing.
* 2 CJW and CJA in "Type" mean cavitating jet in water and air. (P) means the use of pressurized chamber.
3 Value in [] is quoted from the value of same standard material.
* 4 Value in () is required value on the standard.

5.3. Simulation of cavitation peening by using ultrasonic

In the case of cavitation peening using ultrasonic, Jung et al. (2017) simulated the alternative pressure amplitude in a narrow tube, which corresponds to the cavitation intensity, and found it corresponded well with the distribution of residual stress. Bai et al. (2019) simulated the pressure field of bubbly flow in a narrow range for ultrasonic cavitation peening and measured the cavitation intensity by sonoluminescence. Both the experimental and calculated results show that the highest sound pressure is generated when the vibration amplitude is approximately 25 μm and the strongest cavitation intensity occurs at a gap width of 0.5 – 0.7 mm. In shot peening, the pressure distribution can be estimated by the Hertzian contact, or it can be obtained by solid contact with a spherical ball. However, in the case of cavitation impact, the pressure distribution is unknown. Therefore, Lim et al. (2021) assumed the pressure distribution of ultrasonic cavitation peening $p(r, t)$ to be a Lorentzian pressure distribution (see Eq. (6)), and obtained the inverse finite-element (FE) method by measuring the profile of pits induced by ultrasonic cavitation peening using atomic force microscopy (AFM) (see Fig. 31). They concluded that the proposed simulation based

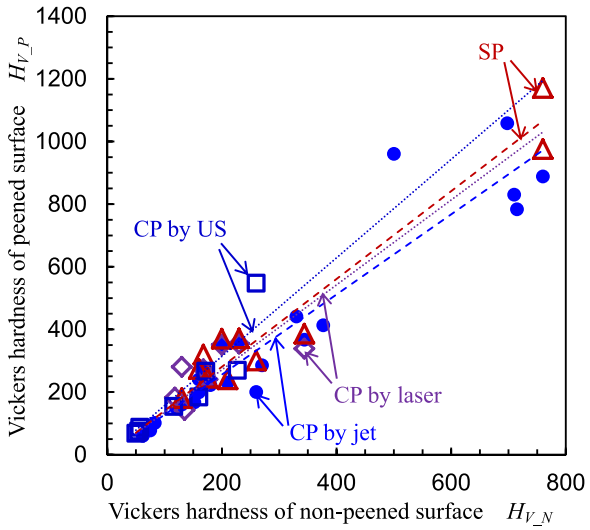

Fig. 23. Relationship of Vickers hardness between non-peened and peened surface.

Table 4
Correlation between Vickers hardness of non-peened surface and that of peened one.

Peening method	Improvement ratio k_{HV}	Correlation coefficient	Number of data set	Probability of non-correlation
CP by jet	128%	0.948	25	7.0×10^{-11}%
CP by laser	136%	0.298	8	47%
CP by US	157%	0.904	8	0.21%
SP	140%	0.973	11	5.3×10^{-5}%

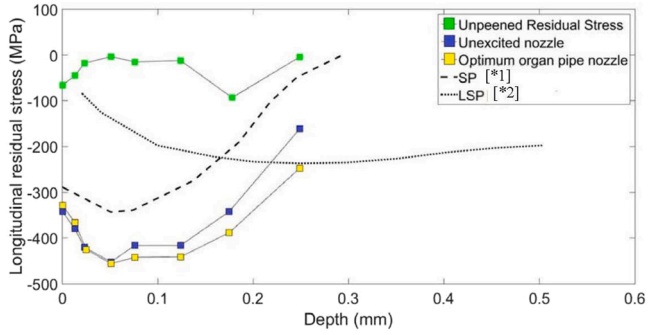

Fig. 24. Distribution of compressive residual stress introduced by cavitation peening comparing with shot peening (aluminum alloy A7075-T651) (Vidvans et al., 2021 ([*1] Benedetti et al., 2009; [*2] Vazquez et al., 2012)).

on the pit profile adequately predicted the growth of the residual stress field with increasing peening time.

$$p(r,\quad t) = \frac{\sigma_p}{\left[1+\left(\frac{r}{r_d}\right)^2\right]^m} \quad \exp\left[-a\quad\left(2\frac{t}{t_d}-1\right)^2\right] \tag{6}$$

Here, σ_p is the magnitude of the maximum pressure, r_d is the characteristic radius, m is the shape parameter, and t_d is the characteristic time. The σ_p, r_d, m, and t_d values were obtained by inverse analysis, as shown in Fig. 31. Note that in the case of cavitation peening by the jet, the diameter of the pit was several hundreds μm for the steel, and several millimeters in aluminum (Soyama, 2017). As the type of cavitation used in the jet is different from that of ultrasonic cavitation, precise

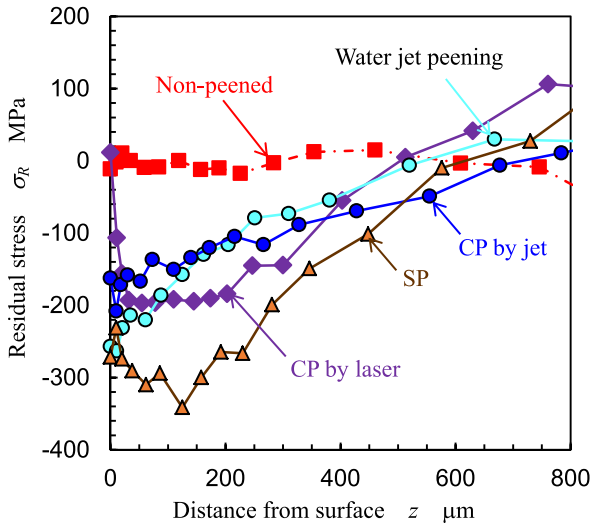

Fig. 25. Distribution of compressive residual stress introduced by cavitation peening comparing with shot peening (austenitic stainless steel SUS316L).

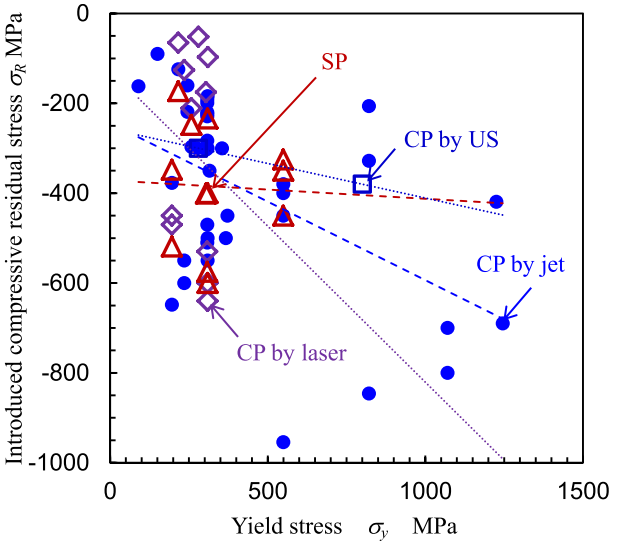

Fig. 26. Compressive residual stress introduced by peening as a function of yield stress of base metal.

Table 5
Correlation between yield stress of base metal and introduced compressive residual stress.

Peening method	Correlation coefficient	Number of data set	Probability of non-correlation
CP by jet	0.497	39	0.13%
CP by laser	0.144	11	67%
CP by US	(1)	2	–
SP	0.041	12	90%

measurement of the pit shape induced by the jet, i.e., vortex cavitation, would be required.

6. Future work of cavitation peening based on reported results

6.1. Fatigue tests and measurements of material properties

As shown in Table 1 and Figs. 20–22, cavitation peening using the

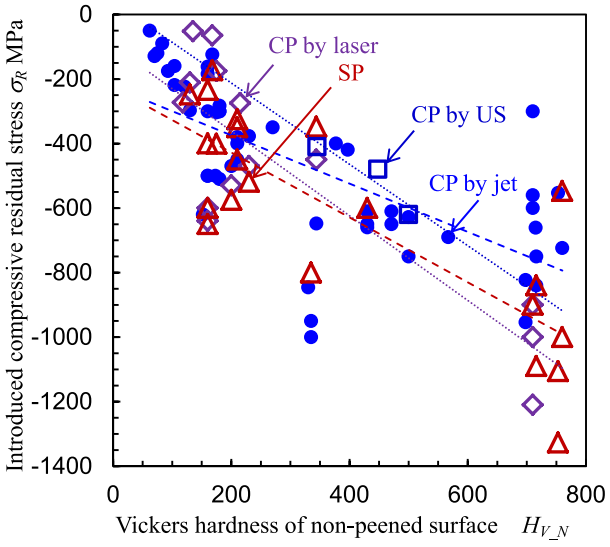

Fig. 27. Compressive residual stress introduced by peening as a function of Vickers hardness of non-peened surface.

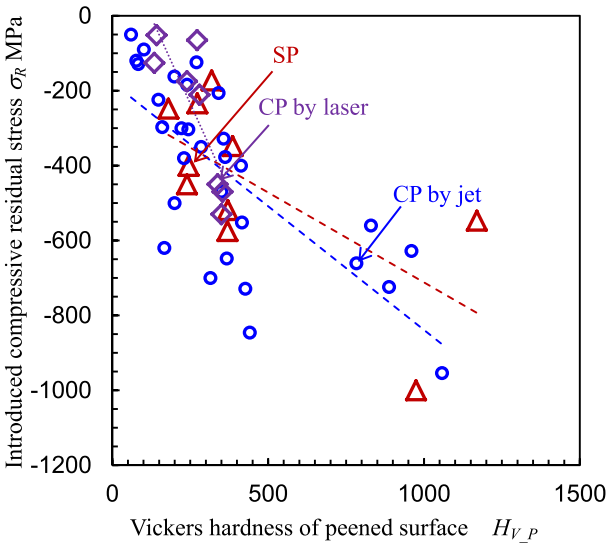

Fig. 28. Relationship between Vickers hardness of peened surface and introduced compressive residual stress.

Table 6
Correlation between Vickers hardness of non-peened surface and introduced compressive residual stress.

Peening method	Correlation coefficient	Number of data set	Probability of non-correlation
CP by jet	0.687	52	1.9×10^{-6}%
CP by laser	0.854	14	0.01%
CP by US	0.929	3	22%
SP	0.814	22	4.1×10^{-4}%

jet, pulsed laser, and ultrasound can improve the fatigue strength as well as shot peening. To elucidate the characteristics of cavitation peening compared with shot peening, further fatigue tests using the same lot of specimens treated by different peening methods would be required. In order to make clear differences on mechanical properties of treated surface between cavitation peening and shot peening, measurement of Vickers hardness, surface roughness, and residual stress are required. The minimum requirement for the mechanical property of the peened

Table 7
Correlation between Vickers hardness of peened surface and introduced compressive residual stress.

Peening method	Correlation coefficient	Number of data set	Probability of non-correlation
CP by jet	0.726	30	5.7×10^{-4}%
CP by laser	0.833	8	1.0%
CP by US	–	–	–
SP	0.679	10	3.1%

specimen is the Vickers hardness. The Vickers hardness of the peened surface included the effects of work hardening and residual stress. It was revealed that the result of the indentation test was affected by the residual stress experimentally and numerically, and they proposed an estimation method for residual stress from the indentation test. Namely, the Vickers hardness of the peened surface includes the effect of residual stress.

Fig. 32 shows the effect of compressive residual stress on the Vickers hardness and Rockwell superficial hardness experimentally. As shown in Fig. 32 (a), when the front surface of the plate specimen was peened, its surface deformed in a convex shape, as the front surface was elongated by plastic deformation due to peening, and the compressive residual stress was introduced at the surface of the backside. As the back side was not peened, the change in hardness revealed the effect of compressive residual stress. Fig. 32 (b) and (c) show the relationship between the residual stress and Vickers hardness $H_{V\ NP}$ and Rockwell superficial hardness $H_{R15T\ NP}$ of the back side, i.e., non-peened surface. The residual stress was measured by the 2D method using XRD (Soyama et al. (2021c). At Vickers hardness $H_{V\ NP}$, the applied load was 9.8 N. Regarding the Rockwell superficial hardness, the preliminary minor load was 29.4 N and the additional major load was 147 N, and a spherical ball with a diameter of 1.59 mm was used. Futakawa et al. (2001) reported an estimation method of elastic-plastic properties by the indentation technique with different indenters, and Cao and Lu (2004) revealed that the plastic properties of metal materials were evaluated by a spherical indentation test. Note that Rockwell superficial hardness has an advantage in the measurement of peened surfaces, as the surface roughness caused by peening can be neglected by applying a preliminary minor load. Fig. 32 (b) and (c) show the Vickers hardness $H_{V\ NP}$ and Rockwell superficial hardness $H_{R15T\ NP}$ as a function of the change in residual stress with peening intensity. As shown in Fig. 32 (b) and (c), both Vickers hardness $H_{V\ NP}$ and Rockwell superficial hardness $H_{R15T\ NP}$ increased with the compressive residual stress σ_R. When the following experimental formulas, i.e., Eqs. (7) and (8), were assumed for the relation between the compressive residual stress σ_R and hardness $H_{V\ NP}$ and $H_{R15T\ NP}$, the constants k_1 and k_2 were 0.035 ± 0.006 and 163.0 ± 1.1 for stainless steel SUS316L, 0.066 ± 0.006 and 143.7 ± 1.1 for duralumin A2024-T3, respectively. The constants k_3 and k_4 were -0.0055 ± 0.0005 and 91.82 ± 0.09, respectively, for duralumin A2024-T3.

$$H_{VNP} = -k_1\,\sigma_R + k_2 \tag{7}$$

$$H_{R15TNP} = -k_3\,\sigma_R + k_4 \tag{8}$$

The correlation coefficient and the probability of non-correlation of the above-mentioned relation were 0.870% and 0.024% for SUS316L of σ_R - $H_{V\ NP}$ and 0.959% and 0.0003% for A2024-T3 of σ_R - $H_{V\ NP}$. Of course, the hardness of the peened surface included the effects of work hardening and compressive residual stress introduced by peening.

Note that the Vickers hardness $H_{V\ NP}$ of duralumin A2024-T3 in Fig. 32 (b) was obtained from Rockwell superficial hardness $H_{R15T\ NP}$ by following procedures, as $H_{V\ NP}$ of duralumin A2024-T3 could not be directly measured using a Vickers hardness tester. Because soft metallic materials such as duralumin were largely deformed, the optical lens and indenter of the conventional Vickers hardness tester could not be

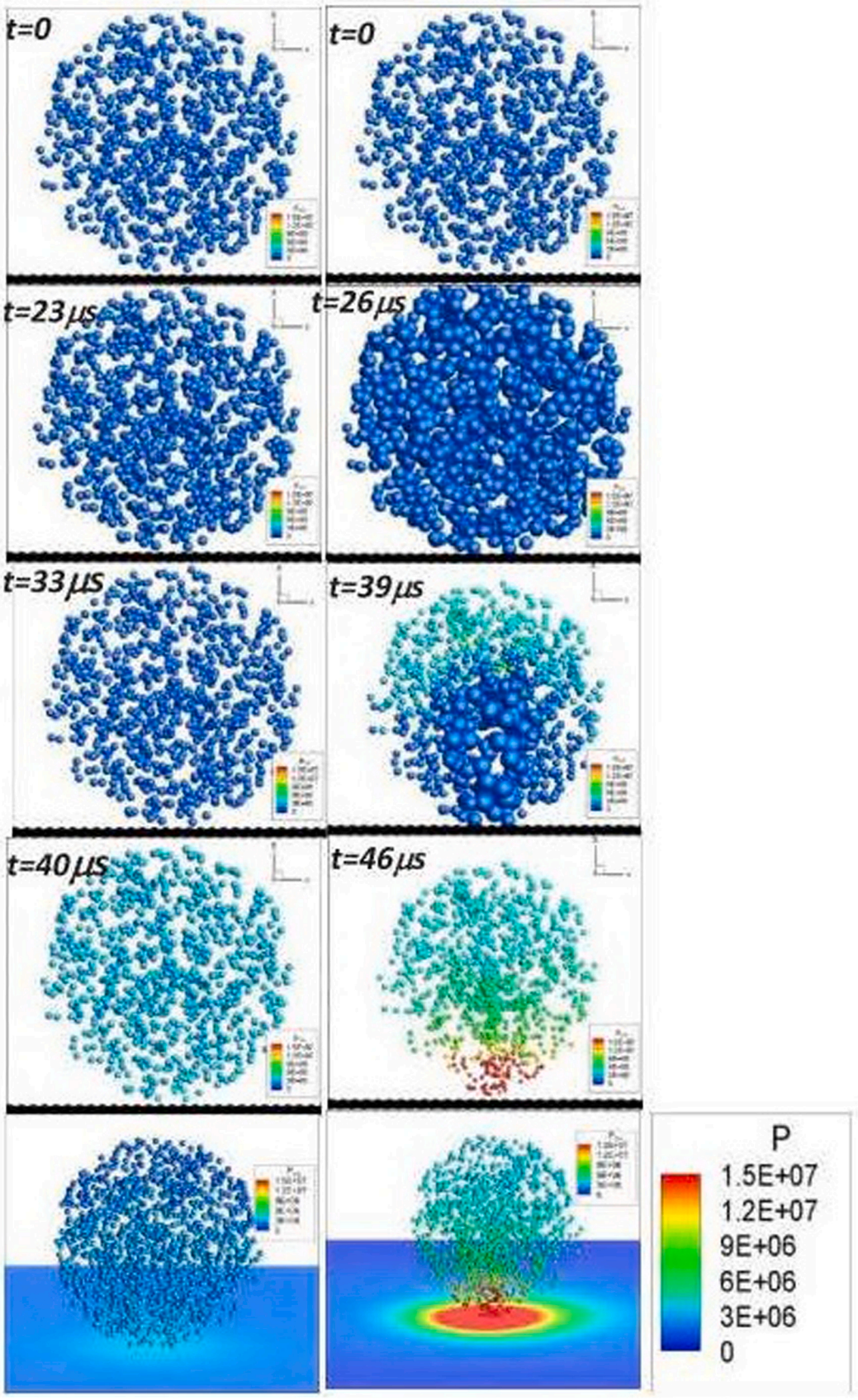

Fig. 29. Time sequence of bubble distributions and internal pressures (indicated by the colored contours) in a bubble cloud driven by pressure excitation with two amplitudes. Left Column: 4 atm and right column: 16 atm The last frame of each row is a view of the pressures at the rigid wall (Ma et al., 2018). (For interpretation of the references to colour in this figure, the reader is referred to the web version of this article.)

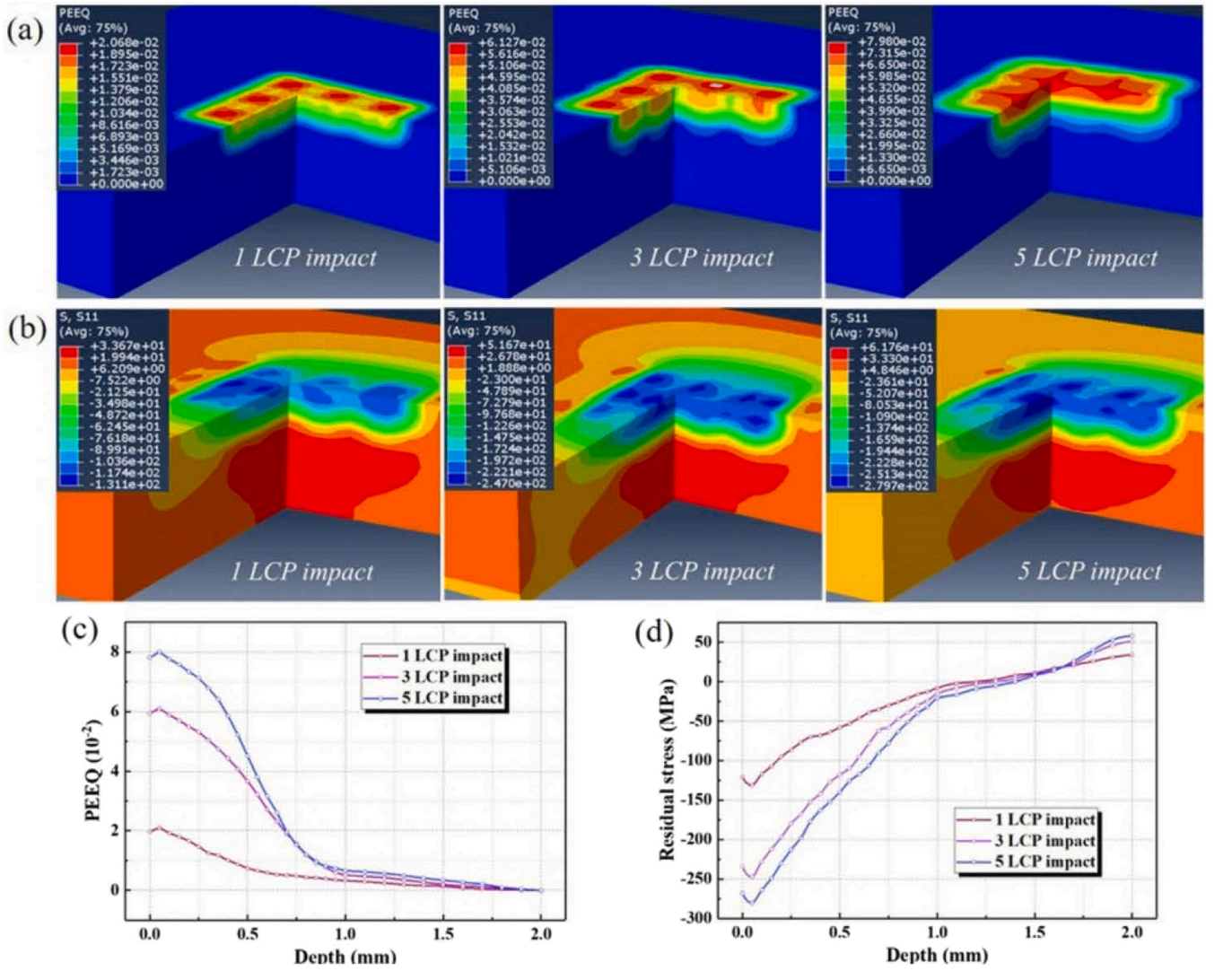

Fig. 30. Simulation of (a) equivalent plastic strain and (b) residual stress field of Q235 steel after the multiple laser cavitation peening impact, value of (c) equivalent plastic strain and (d) residual stress in the direction of depth (Gu et al., 2021a).

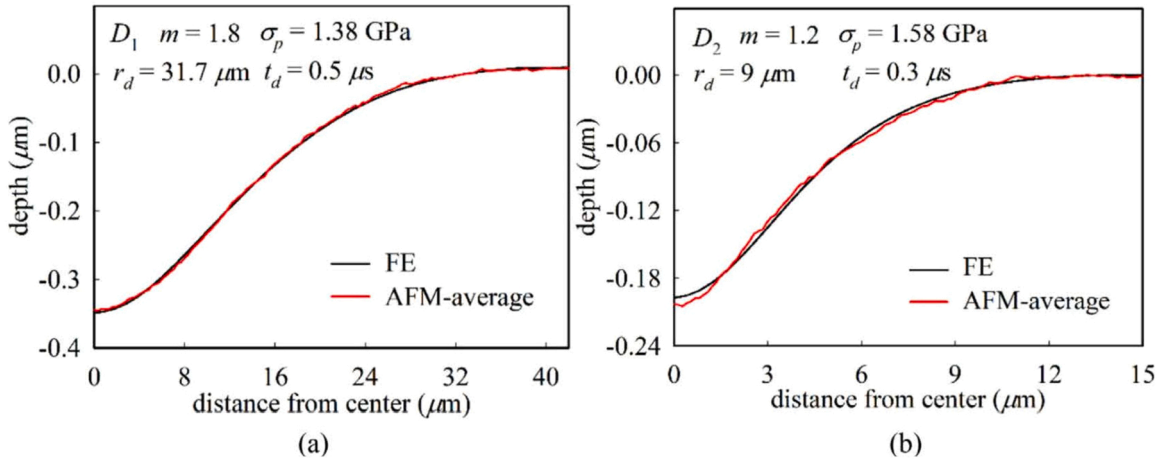

Fig. 31. Pit profile measured by atomic force microscopy (AFM) and estimated by inverse finite-element (FE) induced by ultrasonic cavitation peening impact (Lim et al., 2021).

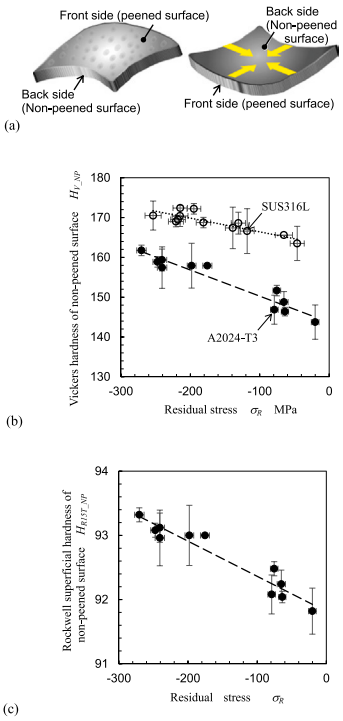

Fig. 32. (a) Schematic diagram of the introduction of compressive residual stress into the back side (non-peened surface). (b) Effect of compressive residual stress on Vickers hardness (SUS316L and A2024-T3). (c) Effect of compressive residual stress on the Rockwell superficial hardness (A2024-T3).

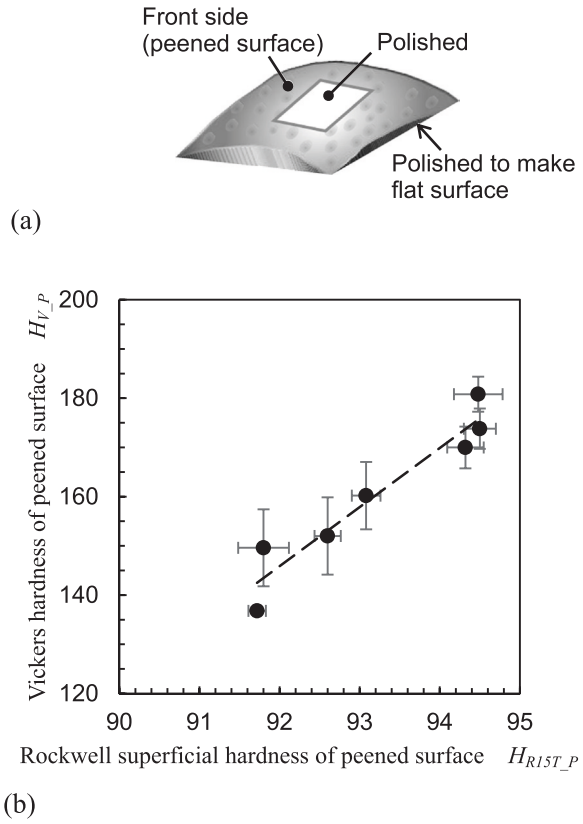

Fig. 33. (a) Schematic of the specimen to obtain the relationship between Rockwell superficial hardness H_{R15T} and Vickers hardness H_V. (b) Relationship between Rockwell superficial hardness $H_{R15T\ P}$ and Vickers hardness $H_{V\ P}$.

switched. Thus, the relationship between Rockwell superficial hardness $H_{R15T\ P}$ and Vickers hardness $H_{V\ P}$ was obtained experimentally by measuring $H_{R15T\ P}$ and $H_{V\ P}$ on the peened surface, as shown in Fig. 33 (a). Fig. 33 (b) illustrates the relationship between $H_{R15T\ P}$ and $H_{V\ P}$. As $H_{V\ P}$ was proportional to $H_{R15T\ P}$, H_V of A2024-T3 was calculated from H_{R15T} using the following equation:

$$H_V = k_5\, H_{R15T} + k_6 \tag{9}$$

Here, k_5 and k_6 are constants, they are 12.0 ± 1.6 and -959 ± 150, respectively. These constants depend on the materials and peening methods used. For reference, the relationship between Rockwell superficial hardness $H_{R15T\ P}$ and Vickers hardness $H_{V\ P}$ of stainless steel SUS316L, which was used in the reference (Soyama, 2019), is shown in Fig. 34. As shown in Fig. 34, $H_{V\ P}$ was roughly proportional to $H_{R15T\ P}$; k_5 and k_6 are 33 ± 6 and -2900 ± 540 for CP by jet, 55 ± 18 and -4900 ± 1600 for CP by laser, and 30 ± 5 and -2580 ± 450 for SP, respectively. Chollacoop et al. (2003) pointed out that two different indenters were required for the evaluation of the yield stress and work-hardening coefficient by indentation tests. Chen et al. (2007) also proposed an estimation method for elastoplastic properties from indentation tests using multiple indenters. In other words, the differences in the relationship of the results using different indenters suggest differences in the material properties. Thus, the surface peened by CP might have different characteristics from those of the shot-peened surface.

As mentioned above, the Vickers hardness includes the effects of work hardening and compressive residual stress introduced by peening. Fig. 35 reveals the relationship between the Vickers hardness of peened surface $H_{V\ P}$ and fatigue strength of peened specimen σ_{fP}, which are shown in Tables 1 and 3. As shown in Fig. 35, σ_{fP} roughly increased with H_{V_P}, thus, Eq. (10), is assumed.

$$\sigma_{fP} = k_7\, H_{VP} + k_8 \tag{10}$$

Here, k_7 *and* k_2 are constants. For all data, that is, non-peened, CP by jet, CP by laser, and SP, k_7 is 1.47 ± 0.23, and k_8 is -17 ± 57. The approximate line is illustrated by the dotted line in Fig. 35. As the correlation coefficient is 0.86 for 17 datasets, the probability of non-correlation is 3.2×10^{-6}%. Namely, the relationship between the Vickers hardness of the peened surface and the fatigue strength of the peened specimen σ_{fP} is highly significant. In the case of non-peened and CP by jet except SP and CP by laser, k_7 was 1.74 ± 0.19, and k_8 was -39 ± 45. The approximate line is illustrated by the dashed-dotted line in Fig. 35. As the correlation coefficient is 0.95 for 12 datasets, the probability of non-correlation is 9.7×10^{-7}%. In other words, the data of non-peened and CP by jet were almost on line. In comparison, the

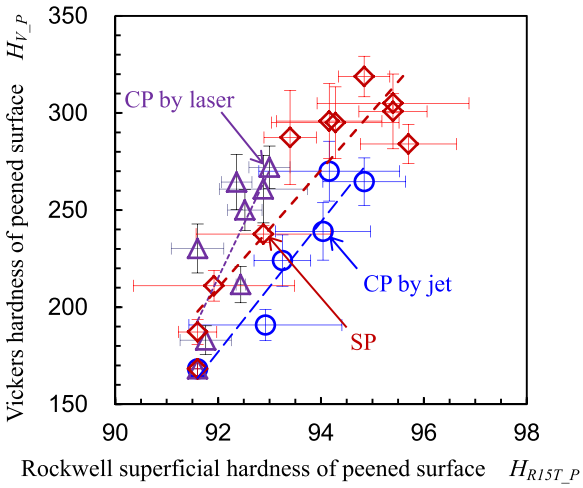

Fig. 34. Relationship between Rockwell superficial hardness $H_{R15T\ P}$ and Vickers hardness $H_{V\ P}$ of SUS316L.

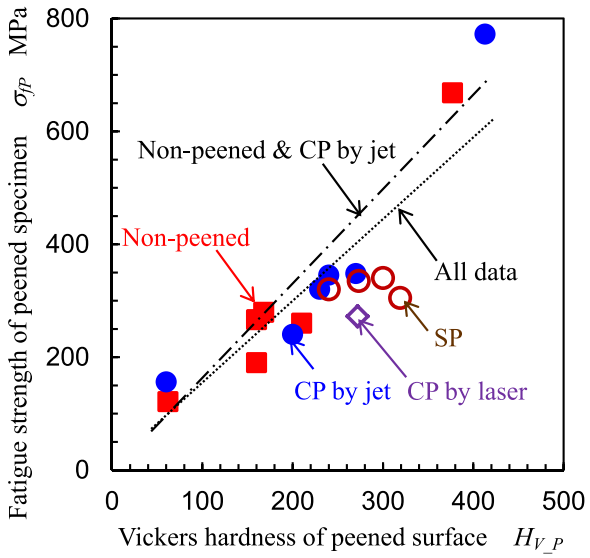

Fig. 35. Relation between Vickers hardness of peened surface and fatigue strength.

hardness of SP, which corresponds to the equivalent fatigue strength of non-peened and CP by jet was harder than that of non-peened and CP by jet. Kumagai et al. (2021) evaluated cavitation-peened specimens by jet and laser compared with shot-peened specimens at equivalent peening intensity by electron backscatter diffraction analysis (EBSD) and diffraction line profile analysis (LPA). They revealed that the dislocation density of shot peening was higher than that of cavitation peening. Fig. 36 shows the EBSD analysis of the cross-section of the specimens: (a) CP by jet, (b) SP, and (c) CP by laser under equivalent peening conditions. As shown in the grain reference orientation deviation (GROD) maps in Fig. 36, the amplitude of the GROD angle on the SP specimen was uniformly high over 80 μm in depth compared with that of CP by jet and laser.

This difference could be caused by the strain speed during the peening process. It was investigated the depth of the dent and the plastic deformation area caused by shot, cavitation, and laser ablation impact, and found that the dent caused by the laser ablation impact was relatively shallower than that of shot impact, and the dent of cavitation impact was between them. As the yield stress increases with the strain rate, the laser ablation impact is a type of shock wave process whose strain speed is much higher than that of shot impact. Thus, the strain rate during the peening process may have caused the difference. It was also evaluated the effect of impact velocity on work hardening on the surface of polycrystalline metals subjected to peening by polycrystal plasticity FE analysis, and found that the deformation progresses preferentially along the grain boundary rather than inside the grain after a large impact. To clarify the mechanism of the difference between cavitation peening and shot peening, future investigations, such as EBSD at equivalent peening intensity condition, are required.

As mentioned in the introduction, the major factors of fatigue strength σ_f other than hardness H are surface roughness R_s and residual stress σ_R. Namely, σ_f can be estimated by a function of H, R_s, and σ_R, as shown in Eq. (11).

$$\sigma_f = f(H, R_s, \sigma_R) \tag{11}$$

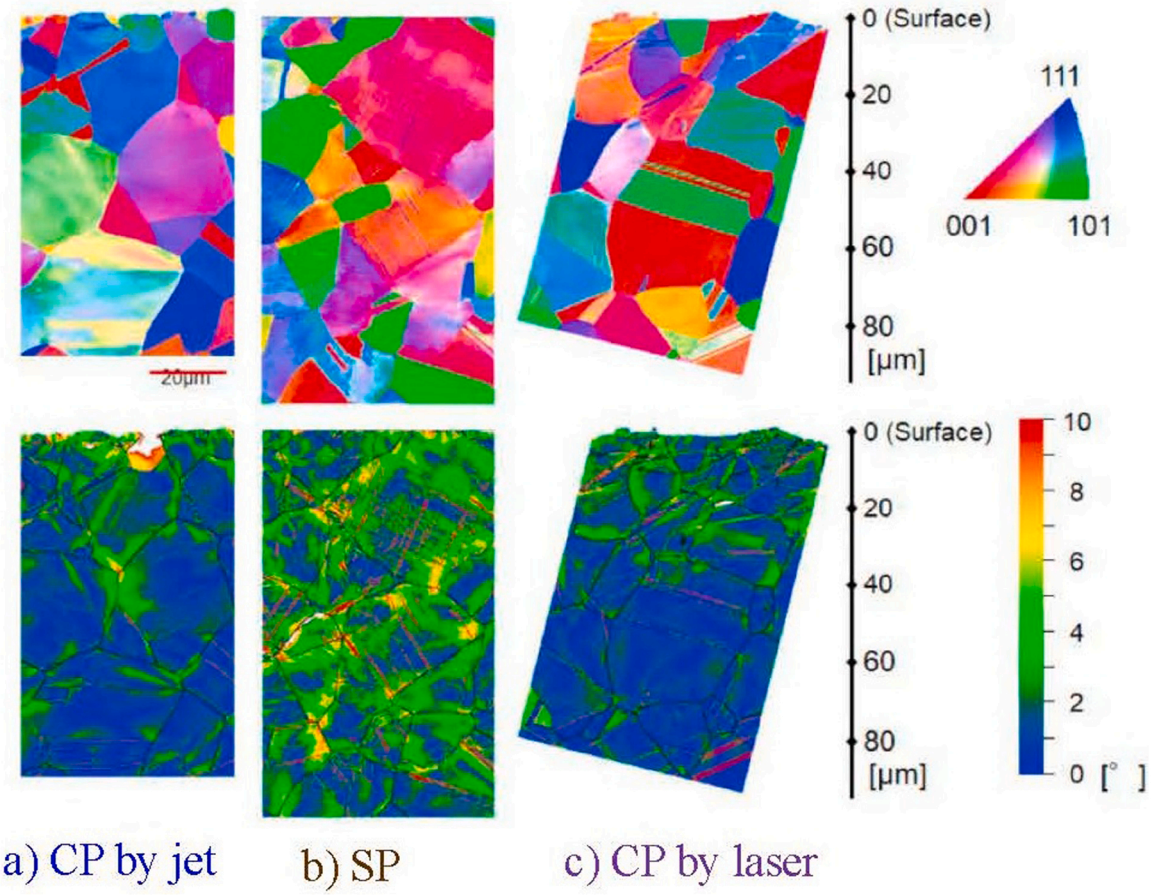

Fig. 36. EBSD analysis of cross-section beneath a) CP by jet, b) SP and c) CP by laser surface treatments showing inverse pole figure maps (top) relative to the normal to the cross-section and grain reference orientation deviation (GROD) maps (bottom) (Kumagai et al. (2021)).

For example, Soyama and Takeo (2020) proposed an estimation method for the fatigue strength $\sigma_{f\,est}$ from the fatigue strength $\sigma_{f\,0}$ at the reference condition using the surface roughness $\Delta Rz'$, surface harness $\Delta H_{R15N}'$, and surface residual stress $\Delta\sigma_R$, as shown in Eq. (12). $\Delta Rz'$ and $\Delta H_{R15N}'$ are the differences in Rz and H_{R15N}, respectively, between the reference condition and the estimated condition and normalized by the reference condition, as shown in Eqs. (13) and (14), respectively. $\Delta\sigma_R$ is the difference in the residual stress between the estimated and reference conditions, as shown in Eq. (15).

$$\sigma_{f\,est} = \sigma_{f0} + a\frac{1}{\Delta Rz'}\sigma_{f0} + b\,\Delta H_{R15N}^{'\,\sigma_{f0}} + c\,\Delta\sigma_R \tag{12}$$

$$\Delta Rz' = \frac{Rz_0 - Rz}{Rz_0} \tag{13}$$

$$\Delta H_{R15N}' = \frac{H_{R15N} - H_{R15N0}}{H_{R15N0}} \tag{14}$$

$$\Delta\sigma_R = \sigma_R - \sigma_{R0} \tag{15}$$

Here, a, b, and c are constants calculated using the least-squares method. In a previous report (Soyama and Takeo, 2020), they were 0.01, 2.59, and − 0.34, respectively.

In the case of the effect of compressive residual stress introduced by peening on the fatigue properties, the relaxation of compressive residual stress should be considered. Zhou et al. (2018) reported the relaxation of compressive residual stress introduced by shot peening and mechanical surface treatment. Telang et al. (2018) investigated the thermal relaxation of compressive residual stresses introduced by mechanical surface treatments, and reported that the relaxation of the cavitation-peened surface was the lowest compared to the other mechanical surface treatments. Kumar et al. (2020) also revealed the relaxation of compressive residual stress introduced by ultrasonic shot peening during a low-cycle fatigue test. Soyama et al. (2021a) investigated the relaxation of compressive residual stress introduced by cavitation peening by the jet compared with that of shot peening during the fatigue test, and it was revealed that the relaxation of cavitation peening was lower than that of shot peening. Therefore, to clarify the characteristics and the effect of residual stress introduced by the cavitation peening on fatigue properties, the residual stress before and after the fatigue test should be measured compared with conventional shot peening.

Considering the above-mentioned characteristics of cavitation peening on fatigue properties, the required measurement of material properties for future experiments on cavitation peening is summarized in Table 8. As the cavitation-peened specimen revealed less hardness at the equivalent fatigue strength compared with the shot-peened specimen, as shown in Fig. 35, the fatigue test is required for the evaluation of fatigue properties of the cavitation-peened specimens. Please do not judge the fatigue properties of cavitation peening by hardness and/or residual stress without a fatigue test. As shown in Tables 1 and 3, the results, which show the comparison of fatigue properties between cavitation peening and shot peening, are very limited. To clarify the differences and advantages of each peening method, a fatigue test of specimens treated by different peening methods is preferred, as the fatigue properties of mechanical surface treatments strongly depend on the virgin materials. In some cases, as it is very difficult to compare the fatigue properties of different lots, please use the same lot to compare the fatigue properties of different mechanical surface treatments. As shown in Fig. 35, the relation between the hardness and fatigue strength shows the characteristics of each peening methods, please measure the hardness such as Vickers hardness and/or Rockwell superficial hardness. Although the applied load of the Rockwell superficial hardness is dozens of times larger than that of the Vickers hardness, the Rockwell superficial hardness shows a peening effect, as shown in Fig. 33 (b) and Fig. 34. The Rockwell superficial hardness also indicates the effect of compressive residual stress, as shown in Fig. 32 (c). As mentioned above, the advantage of Rockwell superficial hardness is that it can reduce the effect of surface roughness by applying a preliminary minor load. When both Vickers hardness and Rockwell superficial hardness were measured, the relationship between both hardness values showed differences in the peening methods, as shown in Fig. 34.

Table 8
Required measurement parameters of materials properties for future experiments of cavitation peening.

Materials properties	Priority
Fatigue life and strength of non-peened and peened specimens (Comparison between different peening methods is preferred)	◎
Hardness of non-peened and peened specimens (Vickers hardness and/or Rockwell superficial hardness)	◎
Residual stress of non-peened and peened specimens (Before and after fatigue test)	○
Surface roughness of non-peened and peened specimens	○
Relation between compressive residual stress and hardness (see Fig. 31)	○
Yield stress	
Tensile strength	
EBSD analysis (Comparison between different peening methods is preferred)	
Evaluation by large scale high energy synchrotron facilities (Comparison between different peening methods is preferred)	

As residual stress is also a major factor of fatigue properties, residual stress data are also useful for predicting fatigue properties (Koster, 1974). As mentioned above, the relaxation of compressive residual stress introduced by peening occurs during fatigue, and the relaxation depends on the peening method. Thus, the measurement of the residual stress before and after the fatigue test is preferred. As mentioned by Mitsubayashi et al. (1995), fatigue properties strongly depend on the residual stress distribution with depth. Thus, the distribution of the residual stress would be useful for understanding and/or estimating the fatigue properties. As shown in Figs. 13 and 25, the maximum compressive residual stress of the cavitation peening by the jet had a maximum at the surface, and that of shot peening had a maximum at a certain depth. As the distribution of residual stress is changed by conditions similar to shot peening (Schiffner and Helling, 1999), the residual stress distribution with depth is also useful data.

The surface roughness inevitably increases due to plastic deformation caused by peening. Bellows and Koster (1972) revealed that the fatigue strength decreased with arithmetic mean roughness R_a at $R_a > 10$ μm. In contrast, it was suggested that the fatigue strength scarcely changed at $R_a < 1$ μm (JSME, 1984). Murakami et al. (1997) reported that the effect of surface roughness can be expressed by an $\sqrt{area}$ parameter. Although Masaki et al. (1999) revealed that the positive effects of peening, such as work hardening and the introduction of compressive residual stress, outweighs the negative effect of increased surface roughness, surface roughness should be reported in the future experimental work on cavitation peening.

When the relationship between the compressive residual stress and hardness, which is obtained by the procedure shown in Fig. 32, is revealed, the relationship can be useful for simple evaluation of the effect of compressive residual stress, as the hardness can express the summation of the distribution of compressive residual stress. As the relationship strongly depends on the material, the relationship should be obtained for each material.

The yield stress and tensile strength are also factors affecting the fatigue properties. As conventional test methods such as tensile tests evaluate the yield stress and tensile strength of bulk material, an inverse analysis using an indention test would be useful to obtain the yield of the surface modification layer. A method to identify the yield stress of metals using micro-indentation tests with a spherical indenter was proposed, and then evaluated the yield stress distribution in the surface layer modified by cavitation peening.

As shown in Fig. 36, EBSD analysis is a powerful tool for investigating the mechanism of plastic deformation caused by peening

methods. To clarify the characteristics of cavitation peening compared to other mechanical surface treatments, EBSD analysis of specimens treated by the other methods is preferred.

Ramadhan et al. (2018) revealed the mapping of residual strain induced by laser peening using neutron transmission spectroscopy, Tomota et al. (2019) reported the dislocation densities and intergranular stresses of plastically deformed austenitic steels by a high-resolution time-of-flight (TOF) neutron diffractometer, Coakley et al. (2020) reported high strain rate deformation and failure of copper by using ultrafast Small-angle X-ray scattering (SAXS) with complementing wide-angle X-ray scattering (WAXS), Lindberg et al. (2021) revealed the differences on macro strain and micro strain of ultrahigh strength steel cut by laser, shearing and milling by using high energy synchrotron radiation. Thus, large scale high energy synchrotron and neutron facilities are useful to investigate macro strain and microstructures of peened surface.

6.2. *Modeling for Simulation*

In the case of shot peening, the boundary condition, that is, the contact condition between the shot and material, is clear, and numerical simulations have been carried out. For example, Meguid et al. (1999) simulated a three-dimensional dynamic FE analysis of shot peening. It is still difficult to simulate the pressure distribution at the bubble collapse at the material surface, even for a spherical bubble. As shown in Fig. 29, Ma et al. (2018) simulated the pressure caused by cloud collapse. However, an actual cavitating jet produces a ring vortex cavitation, as shown in Fig. 6, and a part of the ring collapsed, producing an impact. Although Zhang et al. (2013) simulated the cavitating region of a free cavitating jet, the simulation of an impinging jet was not carried out. Sonde et al. (2018) simulated an impinging cavitating jet; however, their model was that the cavitation in shear around the jet directly hit the impinging surface, and it differed from the actual cavitating jet, as shown in Fig. 6. Thus, macroscopically, a simulation of a cavitating jet that can describe the cloud cavitation and ring cavitation, as shown in Fig. 6, is required for future work to obtain the peening area. In addition, microscopically, a simulation of vortex cavitation collapse is required to simulate the pressure distribution of the impact at bubble collapse, as shown in Fig. 37 (a). It is necessary to evaluate material properties, such as the distribution of residual stress, as the pressure distribution at the impact affects the distribution of residual stress. In addition, the simulation of the vortex cavitation will provide an answer to the question of whether the length of the vortex cavitation corresponds to the diameter of the spherical bubble. As shown in Fig. 5, the vortex cavitation consists of small tiny bubbles, and the collapse of the bubble cloud near the wall was enhanced, as shown in Fig. 29. Thus, the collapse of the vortex cavitation should be analyzed. A combination of the simulation of the impinging cavitating jet and vortex cavitation collapse is preferable, and it is very challenging.

To simulate the residual stress distribution in the surface-modified layer, the pressure distribution at the cavitation collapse is required. Okada et al. (1995) experimentally investigated the intensity and distribution of ultrasonic cavitation collapse impact loads using a magnesium-oxide single crystal, and the pressure distribution at each impact was triangular, as shown in Fig. 37 (a). This pressure distribution at the impact corresponds well to the distribution of the residual stress, which shows the maximum at the surface, as shown in Figs. 13 and 25. One of the best ways to estimate the pressure distribution is by using an inverse FEM by measuring the profile of pits induced by ultrasonic cavitation peening using AFM (see Fig. 31) (Lim et al., 2021). In the case of pits induced by cavitation peening using the jet, the diameter of the pits is in the sub-millimeter and/or millimeter order, as shown in the reference (Soyama, 2017). Thus, the precise measurement of the pits, such as an interference method, which was developed by Pieralli and Tribillon (1987) and applied for the measurement of cavitation erosion pits by Belahadji et al. (1991), is required for future work.

6.3. *Enhancement of cavitation aggressivity*

To reveal the importance of future research on the enhancement of cavitation aggressivity, Fig. 38 shows the relation between the cavitation impact intensity and the frequency of impact of the cavitating jet (Soyama et al., 2011a). The cavitation cloud of the cavitating jet is shedding periodically, with a frequency of several hundred hertz. As shown in Fig. 6, the shedding frequency was approximately 300 Hz and the cloud became the ring vortex cavitation. Subsequently, a part of the ring vortex cavitation collapsed, generating the impacts. This means that one cloud cavitation produces one ring vortex cavitation, and one ring vortex cavitation produces several impacts. Namely, one cloud cavitation produces several impacts. Therefore, several hundred or thousands of impacts would be produced per second. As shown in Fig. 38, the frequency of a small impact is about a thousand per second. Conversely, a relatively large impact such as 120 N was generated one per tens-seconds, or an impact of 150 N was produced one per hundred seconds. If each cloud cavitation produces a large impact, such as 150 N, the efficiency of cavitation peening can be enhanced by a hundred times. Kamisaka and Soyama (2021) revealed that a strong impact force is generated by the interference effect of several cloud cavitations. This result suggests that several cloud cavitations are required for a large

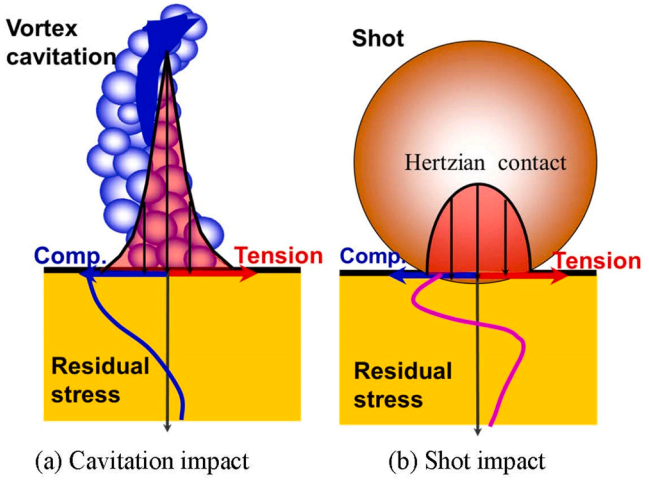

Fig. 37. Schematic diagram of microscopic model of cavitation peening comparing with shot peening.

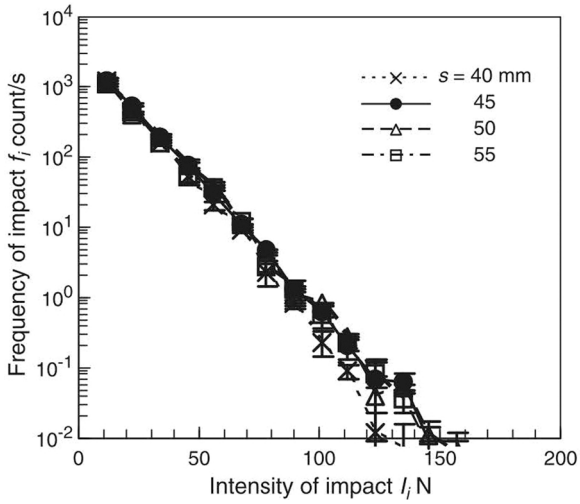

Fig. 38. Relation between intensity and frequency of impact (Soyama et al., 2011a).

impact. Even though several clouds are required for a large impact, the efficiency of the cavitation peening using the jet can be improved by approximately 10 times. The mechanism as to why very few impacts per ten-seconds are produced should be investigated to improve the efficiency of cavitation peening using the jet.

To show that the cavitation peening intensity changes with cavitation number σ, Fig. 39 illustrates the mass loss produced by the cavitating jet as a function of cavitation number (Soyama et al., 2012b). Here, it was assumed that a large mass corresponded to a large cavitation peening intensity, as large impacts caused by the cavitating jet produced large plastic deformation within the incubation period as well as a large mass loss at the steady state erosion stage. As the cavitation number σ is defined by Eq. (1), the downstream pressure p_2 increased with σ at constant injection pressure p_1. In other words, the cavitation peening intensity has a maximum at a certain p_2 at constant p_1. In the case of control of p_2, a valve downstream of a closed-chamber system is sufficient without additional power. In the case of the open chamber, that is, the constant p_2 condition, σ decreases with an increase in p_1. In contrast, the jet power increased with p_1. Namely, the cavitation peening intensity with an increase in p_1 at constant p_2 is affected by the increase in p_1 and the effect of σ. The cavitation peening intensity had a maximum at a certain p_1, as shown in Fig. 10 (b). The sound velocity in the cavitating flow field was measured and it was revealed that the tendency of the aggressive intensity of the hydrodynamic cavitation was quantitatively estimated by considering the sound velocity and the frequency of the vortex cavitation. Meaning, that the aggressive cavitation intensity increases with an increase in p_2 due to an increase in sound velocity, as the void ratio is changed by p_2. In any case, once the mechanism of why the aggressive intensity of the cavitating jet has a maximum at certain σ and/or p_2, the cavitation peening intensity by using the cavitating jet can be enhanced drastically without additional power. This knowledge can be applied to cavitation peening using a pulsed laser and ultrasound.

One way to enhance the peening intensity of cavitation peening using a cavitating jet is the development of the nozzle geometry. Note that the increase in the nozzle diameter is also effective in enhancing the cavitation peening intensity, as shown in the reference (Soyama, 2017); however, the increase in the injection pressure p_1 has a limitation for cavitation peening, as shown in Fig. 10 (b). To show the tendency of the aggressive intensity of the cavitating jet from the various nozzles, Fig. 40 illustrates the relative aggressive intensity of the cavitating jet of the various nozzles. The relative intensity was obtained from the erosion rate and/or arc height of the metallic plate specimen at the optimum standoff distance (Soyama, 2017). Nozzles A, B, C, and D in Fig. 40 are conventional nozzles for the water jet (Soyama, 2013). To enhance the aggressive intensity of the cavitating jet, resonating nozzles for drilling

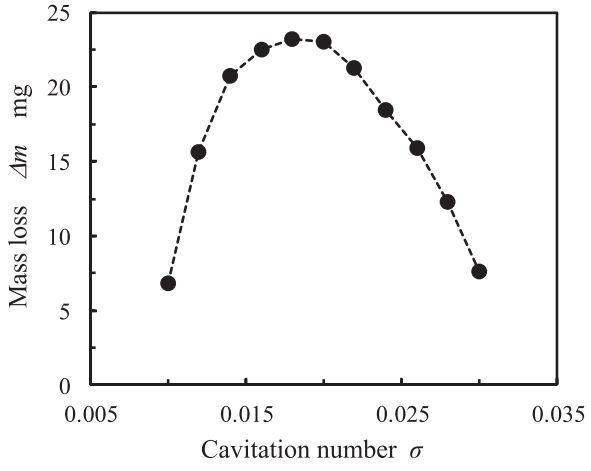

Fig. 39. Mass loss as a function of cavitation number (Soyama et al., 2012b).

were proposed by Johnson et al. (1984) and Chahine and Courbiere (1987), and a horn-type nozzle for peening was proposed. The horn-type nozzle, which was arranged from the conventional water jet nozzle, is shown in Fig. 40 as nozzle E., and Soyama (2011) found that the outlet bore geometry of the nozzle affected the aggressive intensity of the cavitating jet, and he revealed an optimum geometry. During the examination of the repeatability and reproducibility of material testing using a cavitating jet (ASTM, G134, 17, 2017), Soyama (2013) investigated the effect of nozzle geometry on the erosion rate by comparing nozzles for cavitating jets and water jets. Nozzle F is a standard nozzle for material testing (ASTM, G134, 17, 2017). Nozzle G is a nozzle with an optimized outlet bore. Considering the effect of cavitation nuclei from cavitator and vortices on cavitation erosion, Soyama (2014b) proposed a nozzle equipped with a cavitator and a guide pipe, and revealed its optimum geometry (see nozzle H, I, and J). Ijiri et al. (2018) proposed a nozzle with a cyclone structure at the outlet. Yang et al. (2021) investigated the effect of inlet and outlet geometries of the nozzle throat on the property changes of a metallic surface. Kamisaka and Soyama (2021) proposed a long guide pipe nozzle and a water flow hole nozzle near the nozzle outlet (nozzle K and L). The aggressive intensity of nozzle L, which had both a long guide pipe and water flow holes, was approximately 60 times larger than that of the conventional water jet nozzle. The mass loss data of pure aluminum, bronze, nickel 200, low-carbon nickel, and stainless steel, including the repeatability and reproducibility with the details of the nozzle geometry, were explained in ASTM, G134, 17 (2017). One of the best ways to compare the aggressive intensity of the cavitating jet of a developed nozzle in future works is to compare the erosion rate of the developed nozzle and the standard nozzle after obtaining the optimum standoff distance of each nozzle.

7. Conclusions

Cavitation peening is a family of advanced mechanical surface treatment techniques that include cavitating jet, pulsed laser, and ultrasound methods. These are different and distinct from other established methods such as water jet peening, shot peening, and laser shock peening. The differences and peculiarities of each of these methods were critically examined in terms of the mechanisms and material interaction effects. Published data was reviewed and comparisons made with shot peening and water jet peening.

The coverage of the present review can be summarized as follows:

(1) Water jet, pulsed laser, and ultrasonic cavitation peening enhance the fatigue strength and durability of metallic materials. The improvements in the fatigue strength by cavitation peening exceed those by shot peening. The differences in the improvements between cavitation peening and shot peening were most remarkable for soft metallic metals.

(2) The work hardening due to cavitation peening was lower than that due to shot peening at the equivalent fatigue strength condition. The dislocation density after cavitation peening was smaller than that due to shot peening. This difference is likely to be caused by the strain rate during the peening process, and has interesting and important implications for service performance of treated surface.

(3) Future experimental research is required to compare cavitation peening and shot peening of the same material to clarify the advantage of each peening method. The minimum characterization requirement for material properties of fatigue specimens is indentation hardness, including Vickers and/or Rockwell, but also continuously recording indentation testing (CRIT), since these tests can reveal the depth-dependent effects of work hardening and compressive residual stress introduced by peening. Fatigue testing using materials treated by various peening method, e.g. cavitation peeing vs shot peening, are needed to

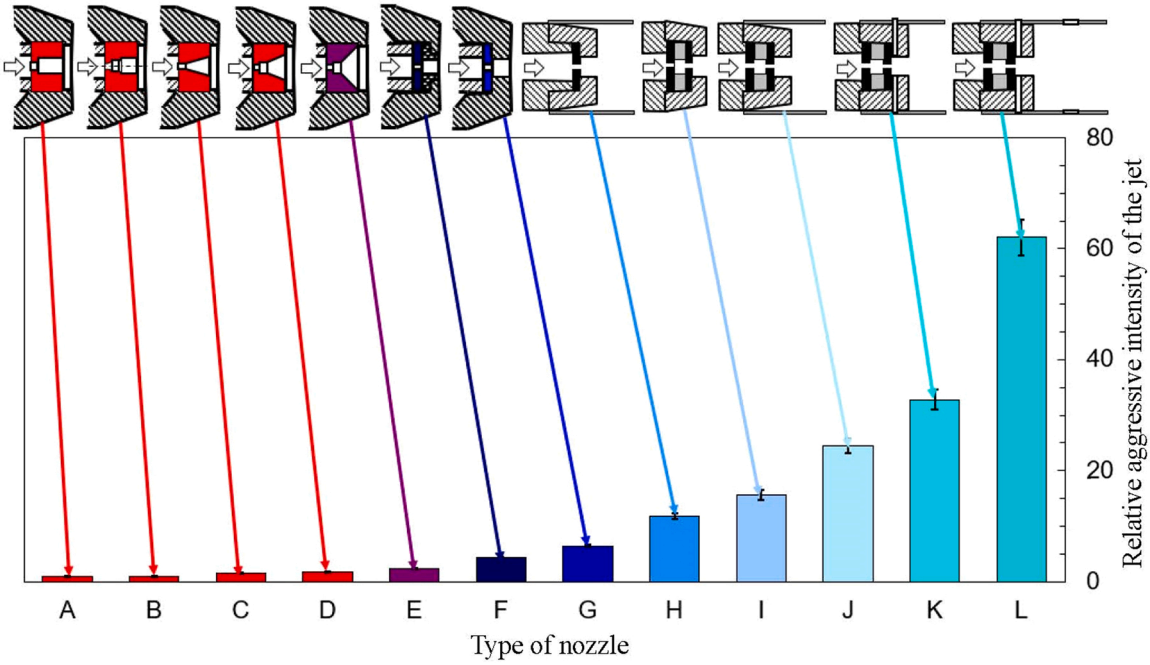

Fig. 40. Relative aggressive intensity of the cavitating jet of various nozzle.

select the most suitable peening method for specific applications. Improvement in the aggressive intensity of cavitation is also expected to enhance the peening effects and increase the efficiency of the process.

(4) Future works on numerical simulation requires the simulation of cloud shedding in the cavitating jet and the collapse of vortex cavitation. From the material modelling point of view, strain rate-dependent elastoplastic analysis is required in which cavitation peening is considered as a type of shock wave process.

(5) When cavitation peening using a submerged high-speed water jet is applied, it is necessary to distinguish between cavitation peening and water jet peening. The classification map for cavitation peening and water jet peening using the optimum standoff distance s_{opt} and cavitation number σ is crucial for distinguishing mechanisms and effects. For cavitation peening using a water jet with an open chamber, the jet at a relatively low injection pressure (i.e., 30 – 40 MPa) using a large nozzle performs better than high injection pressure using a small nozzle. Unlike nozzles for water jet cutting, special nozzles suitable for the cavitating jet can be identified and designed.

CRediT authorship contribution statement

Hitoshi Soyama: Conceptualization, Methodology, Investigation, Writing – original draft, Visualization, Project administration, Funding acquisition. **Alexander M. Korsunsky**: Conceptualization, Writing – review & editing, Supervision.

Declaration of Competing Interest

The authors declare that they have no known competing financial interests or personal relationships that could have appeared to influence the work reported in this paper.

Acknowledgements

This work was partly supported by JSPS KAKENHI Grant Numbers 18KK0103 and 20H03138.

References

ASTM G32–16, 2016. Standard test method for cavitation erosion using vibratory apparatus, ASTM standard, 03.20 1–20.

ASTM G134–17, 2017. Standard test method for erosion of solid materials by a cavitating liquid jet, ASTM standard, 03.02 1–17.

Abramov, V.O., Abramov, O.V., Sommer, F., Gradov, O.M., Smirnov, O.M., 1998. Surface hardening of metals by ultrasonically accelerated small metal balls. Ultrasonics 36 (10), 1013–1019. https://doi.org/10.1016/s0041-624x(98)00027-4.

Ansari, M.A., Abdi Behnagh, R., Salvadori, A., 2020. Numerical analysis of high-speed water jet spot welding using the Arbitrary Lagrangian-Eulerian (ALE) method. Int. J. Adv. Manuf. Technol. 112 (8), 491–504. https://doi.org/10.1007/s00170-020-06358-.

Azhari, A., Schindler, C., Nkoumbou, J., Kerscher, E., 2014. Surface erosion of carbon steel 1045 during waterjet peening. J. Mater. Eng. Perform. 23 (5), 1870–1880. https://doi.org/10.1007/s11665-014-0932-9.

Bagherifard, S., Beretta, N., Monti, S., Riccio, M., Bandini, M., Guagliano, M., 2018. On the fatigue strength enhancement of additive manufactured AlSi10Mg parts by mechanical and thermal post-processing. Mater. Des. 145, 28–41. https://doi.org/10.1016/j.matdes.2018.02.055.

Bagherifard, S., Ghelichi, R., Guagliano, M., 2012. Numerical and experimental analysis of surface roughness generated by shot peening. Appl. Surf. Sci. 258 (18), 6831–6840. https://doi.org/10.1016/j.apsusc.2012.03.111.

Bai, F., Long, Y.Y., Saalbach, K.A., Twiefel, J., 2019. Theoretical and experimental investigations of ultrasonic sound fields in thin bubbly liquid layers for ultrasonic cavitation peening. Ultrasonics 93, 130–138. https://doi.org/10.1016/j.ultras.2018.11.010.

Bai, F.S., Saalbach, K.A., Long, Y.Y., Twiefel, J., Wallaschek, J., 2018a. Capability evaluation of ultrasonic cavitation peening at different standoff distances. Ultrasonics 84, 38–44. https://doi.org/10.1016/j.ultras.2017.10.013.

Bai, F.S., Saalbach, K.A., Wang, L., Wang, X.G., Twiefel, J., 2018b. Impact of time on ultrasonic cavitation peening via detection of surface plastic deformation. Ultrasonics 84, 350–355. https://doi.org/10.1016/j.ultras.2017.12.001.

Bai, F.S., Wang, L., Saalbach, K.A., Twiefel, J., 2018c. A novel ultrasonic cavitation peening approach assisted by water jet. Appl. Sci. 8 (11), 11. https://doi.org/10.3390/app8112218.

Bai, F.S., Wang, L., Yang, K.D., He, Z.Y., Qi, G., Twiefel, J., 2021. Theoretical modeling and experimental investigation of a V-shaped traveling wave piezoelectric transducer for ultrasonic cavitation peening: part B. Appl. Acoust. 178, 10. https://doi.org/10.1016/j.apacoust.2021.107972.

Balamurugan, K., Uthayakumar, M., Gowthaman, S., Pandurangan, R., 2018. A study on the compressive residual stress due to waterjet cavitation peening. Eng. Fail. Anal. 92, 268–277. https://doi.org/10.1016/j.engfailanal.2018.05.012.

Belahadji, B., Franc, J.P., Michel, J.M., 1991. A statistical-analysis of cavitation erosion pits. J. Fluids Eng. 113 (4), 700–706. https://doi.org/10.1115/1.2926539.

Bellows, G., Koster, W.P. ,1972. Surface integrity - update '72: General Electric Company.

Benedetti, M., Fontanari, V., Scardi, P., Ricardo, C.L.A., Bandini, M., 2009. Reverse bending fatigue of shot peened 7075-T651 aluminium alloy: the role of residual

stress relaxation. Int. J. Fatigue 31 (8–9), 1225–1236. https://doi.org/10.1016/j.ijfatigue.2008.11.017.
Blake, J.R., Gibson, D.C., 1987. Cavitation bubbles near boundaries. Annu. Rev. Fluid Mech. 19, 99–123. https://doi.org/10.1146/annurev.fl.19.010187.000531.
Blanken, J., De Moor, R.J.G., Meire, M., Verdaasdonk, R., 2009. Laser induced explosive vapor and cavitation resulting in effective irrigation of the root canal. Part 1: a visualization study. Lasers Surg. Med. 41 (7), 514–519. https://doi.org/10.1002/lsm.20798.
Bregliozzi, G., Schino, A.D., Ahmed, S.I.U., Kenny, J.M., Haefke, H., 2005. Cavitation wear behaviour of austenitic stainless steels with different grain sizes. Wear 258 (1–4), 503–510. https://doi.org/10.1016/j.wear.2004.03.024.
Brennen, C.E., 1995. Cavitation and Bubble Dynamics. Oxford University Press.
Cao, Y.P., Lu, J., 2004. A new method to extract the plastic properties of metal materials from an instrumented spherical indentation loading curve. Acta Mater. 52 (13), 4023–4032. https://doi.org/10.1016/j.actamat.2004.05.018.
Chahine, G.L., Courbiere, P., 1987. Noise and erosion of self-resonating cavitating jets. J. Fluids Eng. 109 (4), 429–435. https://doi.org/10.1115/1.3242684.
Chahine, G.L., Hsiao, C.T., 2015. Modelling cavitation erosion using fluid-material interaction simulations. Interface Focus 5 (5), 20150016. https://doi.org/10.1098/rsfs.2015.0016.
Chahine, G.L., Kapahi, A., Hsiao, C.T., Choi, J.K., 2016. Coupling bubble and material dynamics to model cavitation peening and pitting. J. Fluid Sci. Technol. 11 (4), 15. https://doi.org/10.1299/jfst.2016jfst0023.
Chen, X., Ogasawara, N., Zhao, M.H., Chiba, N., 2007. On the uniqueness of measuring elastoplastic properties from indentation: the indistinguishable mystical materials. J. Mech. Phys. Solids 55 (8), 1618–1660. https://doi.org/10.1016/j.jmps.2007.01.010.
Cheng, X.H., Fisher, J.W., Prask, H.J., Gnaupel-Herold, T., Yen, B.T., Roy, S., 2003. Residual stress modification by post-weld treatment and its beneficial effect on fatigue strength of welded structures. Int. J. Fatigue 25 (9–11), 1259–1269. https://doi.org/10.1016/j.ijfatigue.2003.08.020.
Chollacoop, N., Dao, M., Suresh, S., 2003. Depth-sensing instrumented indentation with dual sharp indenters. Acta Mater. 51 (13), 3713–3729. https://doi.org/10.1016/s1359-6454(03)00186-1.
Clauer, A.H., 2019. Laser shock peening, the path to production. Metals 9 (6). https://doi.org/10.3390/met9060626.
Coakley, J., Higginbotham, A., McGonegle, D., Ilavsky, J., Swinburne, T.D., Wark, J.S., Rahman, K.M., Vorontsov, V.A., Dye, D., Lane, T.J., Boutet, S., Koglin, J., Robinson, J., Milathianaki, D., 2020. Femtosecond quantification of void evolution during rapid material failure. Sci. Adv. 6 (51) https://doi.org/10.1126/sciadv.abb4434.
Crum, L.A., 1979. Surface oscillations and jet development in pulsating bubbles. J. De. Phys. Colloq. 40 (C8), 285–288.
Dabir-Moghaddam, N., Liu, Z., Wu, B.X., 2017. Modeling of the shrinking process of a bubble induced by laser metal ablation in water and experimental verification. J. Appl. Phys. 121 (4), 11. https://doi.org/10.1063/1.4973621.
Daniewicz, S.R., Cummings, S.D., 1999. Characterization of a water peening process. J. Eng. Mater. Technol. 121 (3), 336–340. https://doi.org/10.1115/1.2812383.
Delosrios, E.R., Walley, A., Milan, M.T., Hammersley, G., 1995. Fatigue-crack initiation and propagation on shot-peened surfaces in A316 stainless-steel. Int. J. Fatigue 17 (7), 493–499. https://doi.org/10.1016/0142-1123(95)00044-t.
Dominguez Cortazar, M.A., Franc, J.P., Michel, J.M., 1997. The erosive axial collapse of a cavitating vortex: an experimental study. J. Fluids Eng. 119 (3), 686–691. https://doi.org/10.1115/1.2819299.
Enomoto, K., Hirano, K., Mochizuki, M., Kurosawa, K., Saito, H., Hayashi, E., 1996. Improvement of residual stress on material surface by water jet peening. J. Soc. Mater. Soc., Jpn. 45 (7), 734–739.
Fukuda, S., Matsui, K., Ishigami, H., Amano, T., Takahashi, K., Ando, K., 2008a. Improvement of bending fatigue limit by cavitation peening for carbon steel specimens containing an artificial surface defect, Proceeding of 10th International Conference on Shot Peening 116–120.
Fukuda, S., Matsui, K., Ishigami, H., Ando, K., 2008b. Cavitation peening to improve the fatigue strength of nitrocarburized steel. Fatigue Fract. Eng. Mater. Struct. 31 (10), 857–862. https://doi.org/10.1111/j.1460-2695.2008.01273.x.
Futakawa, M., Wakui, T., Tanabe, Y., Ioka, I., 2001. Identification of the constitutive equation by the indentation technique using plural indenters with different apex angles. J. Mater. Res. 16 (8), 2283–2292. https://doi.org/10.1557/jmr.2001.0314.
Gao, Y.B., Wu, B.X., Liu, Z., Zhou, Y., Shen, N.G., Ding, H.T., 2014. Ultrasonic cavitation peening of stainless steel and nickel alloy. J. Manuf. Sci. Eng. 136 (1), 014502 https://doi.org/10.1115/1.4025756.
Gill, A., Telang, A., Mannava, S.R., Qian, D., Pyoun, Y.-S., Soyama, H., Vasudevan, V.K., 2013. Comparison of mechanisms of advanced mechanical surface treatments in nickel-based superalloy. Mater. Sci. Eng.: A 576, 346–355. https://doi.org/10.1016/j.msea.2013.04.021.
Gogate, P.R., Kabadi, A.M., 2009. A review of applications of cavitation in biochemical engineering/biotechnology. Biochem. Eng. J. 44 (1), 60–72. https://doi.org/10.1016/j.bej.2008.10.006.
Grinspan, A.S., Gnanamoorthy, R., 2007. Effect of nozzle-traveling velocity on oil cavitation jet peening of aluminum alloy, AA6063-T6. J. Eng. Mater. Technol. 129 (4), 609–613. https://doi.org/10.1115/1.2772339.
Gu, J.Y., Luo, C.H., Ma, P.C.A., Xu, X.C., Wu, Y., Ren, X.D., 2021a. Study on processing and strengthening mechanisms of mild steel subjected to laser cavitation peening. Appl. Surf. Sci. 562, 13. https://doi.org/10.1016/j.apsusc.2021.150242.
Gu, J.Y., Luo, C.H., Lu, Z.B., Ma, P.C., Xu, X.C., Ren, X.D., 2021b. Bubble dynamic evolution, material strengthening and chemical effect induced by laser cavitation peening. Ultrason. Sonochem. 72, 13. https://doi.org/10.1016/j.ultsonch.2020.105441.
Gu, J.Y., Luo, C.H., Zhang, P.H., Ma, P.C., Ren, X.D., 2020. Laser cavitation peening of gray cast iron: effect of coverage layer on the surface integrity. Appl. Surf. Sci. 521, 9. https://doi.org/10.1016/j.apsusc.2020.146295.
Guechichi, H., Castex, L., 2006. Fatigue limits prediction of surface treated materials. J. Mater. Process. Technol. 172 (3), 381–387. https://doi.org/10.1016/j.jmatprotec.2005.10.010.
Gurrutxaga–Lerma, B., Verschueren, J., Sutton, A.P., Dini, D., 2020. The mechanics and physics of high-speed dislocations: a critical review. Int. Mater. Rev. 66 (4), 215–255. https://doi.org/10.1080/09506608.2020.1749781.
Han, B., Ju, D.Y., Jia, W.P., 2007. Influence of water cavitation peening with aeration on fatigue behaviour of sae1045 steel. Appl. Surf. Sci. 253 (24), 9342–9346. https://doi.org/10.1016/j.apsusc.2007.05.076.
Han, B., Ju, D.Y., Yu, X.G., 2010. Combined finite element method and dislocation density method solution to residual stress induced by water cavitation peening, Materials & Design, 31 (7), 3317–3323, 10.1016/j.matdes.2010.02.004.
Han, B., Wang, Y.H., Xu, C.L. , 2013, Jun 22–23). Numerical simulation of residual stress field induced by water-jet cavitation peening. Paper presented at the 3rd International Conference on Mechanical Engineering, Industry and Manufacturing Engineering (MEIME 2013), Wuhan, PEOPLES R CHINA.
He, P.Y., Li, F.Z., Guo, J., Chen, S.S., Guo, Y.Q., Wang, Y., Tan, Z.R., 2021. Research on the water cavitation peening process and mechanism of TC4 titanium alloy. Int. J. Adv. Manuf. Technol. 112 (5–6), 1259–1269. https://doi.org/10.1007/s00170-020-06566-2.
Hirano, K., Enomoto, K., Hayashi, E., Kurosawa, K., 1996. Effect of water jet peening on corrosion resistance and fatigue strength of type 304 stainless steel. J. Soc. Mater. Soc., Jpn. 45 (7), 740–745.
Holkar, C.R., Jadhav, A.J., Pinjari, D.V., Mahamuni, N.M., Pandit, A.B., 2016. A critical review on textile wastewater treatments: possible approaches. J. Environ. Manag. 182, 351–366. https://doi.org/10.1016/j.jenvman.2016.07.090.
Ijiri, M., Shimonishi, D., Kakagawa, D., Yoshimura, T., 2018. New water jet cavitation technology to increase number and size of cavitation bubbles and its effect on pure al surface. Int. J. Lightweight Mater. Manuf. 1, 12–20. https://doi.org/10.1016/j.ijlmm.2018.03.003.
Ijiri, M., Shimonishi, D., Tani, S., Okada, N., Yamamoto, M., Nakagawa, D., Tanaka, K., Yoshimura, T., 2019. Multifunction cavitation technology to improve the surface function of Al – Cu alloy. Int. J. Lightweight Mater. Manuf. 2 (1), 50–56.
Janka, S., Milos, M., Jan, H. ,2016, Nov 15–18). The improvement of the surface hardness of stainless steel and aluminium alloy by ultrasonic cavitation peening. Paper presented at the 11th International Conference on Experimental Fluid Mechanics (EFM), Marienbad, CZECH REPUBLIC.
Johnson, V.E., Chahine, G.L., Lindenmuth, W.T., Conn, A.F., Frederick, G.S., Giacchino, G.J., 1984. Cavitating and structured jets for mechanical bits to increase drilling rate, 1. Tehory Concepts, J. Energy Resour. Technol. 106 (2), 282–288.
JSME,1984. JSME data book: Fatigue of metals 2nd edition (Vol. 2).
Ju, D.Y., Han, B., 2009. Investigation of water cavitation peening-induced microstructures in the near-surface layer of pure titanium. J. Mater. Process. Technol. 209 (10), 4789–4794. https://doi.org/10.1016/j.jmatprotec.2008.12.006.
Jung, S., Prabhu, M., Lee, H., 2017. Peening narrow nozzles of reactor pressure vessels using ultrasonic cavitation. J. Mech. Sci. Technol. 31 (11), 5279–5283. https://doi.org/10.1007/s12206-017-1021-4.
Jung, S., Prabhu, M., Lee, H., 2018. Peening the tip of a notch using ultrasonic cavitation. Ultrasonics 82, 322–326. https://doi.org/10.1016/j.ultras.2017.09.004.
Kahlin, M., Ansell, H., Basu, D., Kerwin, A., Newton, L., Smith, B., Moverare, J.J., 2020. Improved fatigue strength of additively manufactured ti6al4v by surface post processing. Int. J. Fatigue 134, 12. https://doi.org/10.1016/j.ijfatigue.2020.105497.
Kamisaka, H., Soyama, H., 2018. Effect of injection pressure on mechanical surface treatment using a submerged water jet. J. Jet. Flow. Eng. 33 (2), 4–10.
Kamisaka, H., Soyama, H., 2021. Enhancing the aggressive intensity of a cavitating jet by introducing water flow holes and a long guide pipe. J. Fluids Eng. 143 (3), 031201 https://doi.org/10.1115/1.4048683.
Kaufman, J., Racek, J., Cieslar, M., Minárik, P., Steiner, M.A., Mannava, S.R., Vasudevan, V.K., Sharma, A., Böhm, M., Brajer, J., Pilař, J., Pína, L., Mocek, T., 2022. The effect of laser shock peening with and without protective coating on intergranular corrosion of sensitized AA5083. Corros. Sci. 194. https://doi.org/10.1016/j.corsci.2021.109925.
Keller, S., Chupakhin, S., Staron, P., Maawad, E., Kashaev, N., Klusemann, B., 2018. Experimental and numerical investigation of residual stresses in laser shock peened AA2198. J. Mater. Process. Technol. 255, 294–307. https://doi.org/10.1016/j.jmatprotec.2017.11.023.
Kienzler, A., Schulze, V., Lohe, D., 2008. Surface conditioning by ultrasonic wet peening. Proc. 10th Int. Conf. Shot Peen. 205–210.
Kikuchi, K., Ahmed, S.M., Hiraiwa, T., Ito, Y., Oba, R., 1991. An indirect vibratory method capable of simulating several cavitating states JSME. Int. J. Ser. B 34 (1), 1–8.
Kleinbreuer, W., 1976. Werkstoffzerstorung durch kavitation in olhydralishen systemen. Ind. Anz. 98 (61), 1096–1100.
Kleinbreuer, W., 1977. Kavitationserosion in hydraulischen systemen. Ind. -Anz. 99 (34), 609–613.
Klumpp, A., Lienert, F., Dietrich, S., Soyama, H., Schulze, V., 2017. Surface strengthening of AISI4140 by cavitation peening. Proc. 13th Int. Conf. Shot Peen. 440–445.
Kokubun, T., Soyama, H., 2017. Evaluation of fatigue crack propagation in surface modification layer of duralumin treated by various peening. Trans. JSME 83 (853), 1–15. https://doi.org/10.1299/transjsme.18-00161.

Koster, W.P., 1974. Surf. Integr. Mach. Mater.
Kumagai, M., Curd, M.E., Soyama, H., Ungár, T., Ribárik, G., Withers, P.J., 2021. Depth-profiling of residual stress and microstructure for austenitic stainless steel surface treated by cavitation, shot and laser peening. Mater. Sci. Eng. A 813 (141037), 1–8. https://doi.org/10.1016/j.msea.2021.141037.
Kumagai, N., Takakuwa, O., Soyama, H., 2016. Improvement of delayed fracture resistance on chrome molybdenum steel bolt by cavitation peening, Trans. JSME, 82, paper No. 16–00111 (842), 1–13.
Kumar, C.S., Chattopadhyay, K., Singh, V., Mahobia, G.S., 2020. Enhancement of low-cycle fatigue life of high-nitrogen austenitic stainless steel at low strain amplitude through ultrasonic shot peening. Mater. Today Commun. 25, 12. https://doi.org/10.1016/j.mtcomm.2020.101576.
Latchoumi, T.P., Balamurugan, K., Dinesh, K., Ezhilarasi, T.P., 2019. Particle swarm optimization approach for waterjet cavitation peening. Measurement 141, 184–189. https://doi.org/10.1016/j.measurement.2019.04.040.
Lee, H., Mall, S., Soyama, H., 2009. Fretting fatigue behavior of cavitation shotless peened Ti–6Al–4V. Tribology Lett. 36 (2), 89–94. https://doi.org/10.1007/s11249-009-9463-1.
Lesyk, D.A., Soyama, H., Mordyuk, B.N., Dzhemelinskyi, V.V., Martinez, S., Khripta, N.I., Lamikiz, A., 2019. Mechanical surface treatments of AISI304 stainless steel: effects on surface microrelief, residual stress, and microstructure. J. Mater. Eng. Perform. 28 (9), 5307–5322. https://doi.org/10.1007/s11665-019-04273-y.
Li, F.Z., Guo, J., Chen, S.S., Guo, Y.Q., Li, R.T., Wang, Y., Tan, Z.R., He, P.Y., 2021. Influence law and optimization analysis of technological parameters of TC4 titanium alloy on water cavitation peening. Proc. Inst. Mech. Eng. Part B-J. Eng. Manuf. 8. https://doi.org/10.1177/09544054211041070.
Lichtarowicz, A., 1979. Cavitating jet apparatus for cavitation erosion testing, erosion: prevention and useful applications. ASTM STP 669, 530–549.
Lichtarowicz, A., Scott, P.J., 1979. Erosion testing with cavitating jet, Proceedings of 5th International Conference on Erosion by Liquid and Solid Impact, paper No. 69.
Lim, Y., Murugesan, P., Jung, S., Lee, H., 2021. Evaluation of residual stress from ultrasonic cavitation peening using cavitation pit analysis and fea. Int. J. Mech. Sci. 198, 11. https://doi.org/10.1016/j.ijmecsci.2021.106352.
Lindberg, F., Ryde, L., Brask, J., Hörnström, S.E., Östberg, J., Müller, T., 2021. Stress mapping on ultrahigh strength steel cut edges. Adv. Eng. Mater. 23 (11) https://doi.org/10.1002/adem.202001168.
Liu, B.S., Ma, F., 2021. Erosion behavior of aluminum by an inclined cavitating jet. Wear 474, 15. https://doi.org/10.1016/j.wear.2021.203751.
Liu, G., Lu, J., Lu, K., 2000. Surface nanocrystallization of 316L stainless steel induced by ultrasonic shot peening. Mater. Sci. Eng. A 286 (1), 91–95. https://doi.org/10.1016/s0921-5093(00)00686-9.
Lu, H., Wang, Z., Cai, J., Xu, X., Luo, K., Wu, L., Lu, J., 2021. Effects of laser shock peening on the hot corrosion behaviour of the selective laser melted Ti6Al4V titanium alloy. Corros. Sci. 188. https://doi.org/10.1016/j.corsci.2021.109558.
Lu, H.F., Luo, K.Y., Wu, L.J., Cui, C.Y., Lu, J.Z., 2019. Effects of service temperature on tensile properties and microstructural evolution of CP titanium subjected to laser shock peening. J. Alloy. Compd. 770, 732–741. https://doi.org/10.1016/j.jallcom.2018.08.161.
Lu, J., Lu, H., Xu, X., Yao, J., Cai, J., Luo, K., 2020. High-performance integrated additive manufacturing with laser shock peening –induced microstructural evolution and improvement in mechanical properties of Ti6Al4V alloy components. Int. J. Mach. Tools Manuf. 148. https://doi.org/10.1016/j.ijmachtools.2019.103475.
Lu, J.Z., Wu, L.J., Sun, G.F., Luo, K.Y., Zhang, Y.K., Cai, J., Cui, C.Y., Luo, X.M., 2017. Microstructural response and grain refinement mechanism of commercially pure titanium subjected to multiple laser shock peening impacts. Acta Mater. 127, 252–266. https://doi.org/10.1016/j.actamat.2017.01.050.
Lv, J., Luo, K., Lu, H., Wang, Z., Liu, J., Lu, J., 2022. Achieving high strength and ductility in selective laser melting Ti-6Al-4V alloy by laser shock peening. J. Alloy. Compd. 899. https://doi.org/10.1016/j.jallcom.2021.163335.
Ma, J.S., Hsiao, C.T., Chahine, G.L., 2018. Numerical study of acoustically driven bubble cloud dynamics near a rigid wall. Ultrason. Sonochem. 40, 944–954. https://doi.org/10.1016/j.ultsonch.2017.08.033.
Marcon, A., Melkote, S.N., Castle, J., Sanders, D.G., Yoda, M., 2016. Effect of jet velocity in co-flow water cavitation jet peening. Wear 360, 38–50. https://doi.org/10.1016/j.wear.2016.03.027.
Marcon, A., Melkote, S.N., Yoda, M., 2018. Effect of nozzle size scaling in co-flow water cavitation jet peening. J. Manuf. Process. 31, 372–381. https://doi.org/10.1016/j.jmapro.2017.12.002.
Masaki, K., Ochi, Y., Soyama, H., 2008. Fatigue property improvement of type 316L steel by cavitation shotless peening, Proceeding of 10th International Conference on Shot Peening paper No. 053.
Masaki, K., Tohmyoh, Y., Ochi, Y., Matsumura, T., 1999. The effect of hard shot-peening on high cycle fatigue properties of SUS316L steel: evaluation of surface roughness effects using the annealing method. Trans. JSME 65A (630), 334–339.
Mathias, M., Gocke, A., Pohl, M., 1991. The residual-stress, texture and surface changes in steel induced by cavitation. Wear 150 (1–2), 11–20. https://doi.org/10.1016/0043-1648(91)90302-b.
Meguid, S.A., Shagal, G., Stranart, J.C., Daly, J., 1999. Three-dimensional dynamic finite element analysis of shot-peening induced residual stresses. Finite Elem. Anal. Des. 31 (3), 179–191. https://doi.org/10.1016/s0168-874x(98)00057-2.
Miao, H.Y., Demers, D., Larose, S., Perron, C., Levesque, M., 2010. Experimental study of shot peening and stress peen forming, Journal of Materials Processing Technology, 210 (15), 2089–2102, 10.1016/j.jmatprotec.2010.07.016.
Mitsubayashi, M., Miyata, T., Aihara, H., 1995. Prediction of improvement in fatigue strength by shot peening and selection of most effective peening condition. Trans. JSME 61A (586), 1172–1178.
Momma, T., Lichtarowicz, A., 1995. A study of pressure and erosion produced by collapsing cavitation. Wear 186 (2), 425–436. https://doi.org/10.1016/0043-1648(95)07144-x.
Murakami, Y., Takahashi, K., Yamashita, T., 1997. Quantitative evaluation of the effect of surface roughness on fatigue strength: effect of depth and pitch of roughness. Trans. JSME 63 (612), 1612–1619.
Nakagawa, M., Watanabe, T., 2004. Introducing compressive residual stress on metal surfaces by irradiating ultrasonic wave with a horn in water: Surface modification by irradiating ultrasonic wave in liquid (report 1), Quarterly. J. Jpn. Weld. Soc. 22 (4), 587–594.
Nobel, A.J., Talmon, A.M., 2012. Measurements of the stagnation pressure in the center of a cavitating jet. Exp. Fluids 52 (2), 403–415. https://doi.org/10.1007/s00348-011-1231-y.
Odhiambo, D., Soyama, H., 2003. Cavitation shotless peening for improvement of fatigue strength of carbonized steel. Int. J. Fatigue 25 (9–11), 1217–1222. https://doi.org/10.1016/s0142-1123(03)00121-x.
Ogawa, M., 2014. Development and commercialization of advanced cleaning system for skin pass mill work roll, type cavitating jet in air: Realization of high-quality and high-productivity in hot dip continuous galvanizing line. In: Technical Review, 5. Nippon Steel & Sumikin Engineering Co., Ltd.,, pp. 14–20.
Ohya, T., Okimura, K., Ohta, T., Ichioka, T., 2000. Residual stress improved by water jet peening for small-diameter pipe inner surfaces, Mitsubishi Heavy Industries, Ltd. Tech. Rev. 37 (2), 52–55.
Okada, T., Hattori, S., Shimizu, M., 1995. A fundamental-study of cavitation erosion using a magnesium-oxide single crystal (intensity and distribution of bubble collapse impact loads). Wear 186 (2), 437–443. https://doi.org/10.1016/0043-1648(95)07162-8.
Okura, Y., Sasaki, H., Soyama, H., 2020. Effect of mechanical properties on fatigue life enhancement of additive manufactured titanium alloy treated by various peening methods, Advanced Surface Enhancement, INCASE 2019, Lecture Notes in. Mech. Eng. 76–87. https://doi.org/10.1007/978-981-15-0054-1_10.
Peng, G.Y., Shimizu, S., 2013. Progress in numerical simulation of cavitating water jets. J. Hydrodyn. 25 (4), 502–509. https://doi.org/10.1016/s1001-6058(11)60389-3.
Peng, G.Y., Yang, C.X., Oguma, Y., Shimizui, S., 2016. Numerical analysis of cavitation cloud shedding in a submerged water jet. J. Hydrodyn. 28 (6), 986–993. https://doi.org/10.1016/s1001-6058(16)60700-x.
Peyre, P., Fabbro, R., Merrien, P., Lieurade, H.P., 1996. Laser shock processing of aluminium alloys. Appl. High. Cycle Fatigue Behav., Mater. Sci. Eng. A 210 (1–2), 102–113. https://doi.org/10.1016/0921-5093(95)10084-9.
Peyre, P., Sollier, A., Chaieb, I., Berthe, L., Bartnicki, E., Braham, C., Fabbro, R., 2003. FEM simulation of residual stresses induced by laser peening. Eur. Phys. J. -Appl. Phys. 23 (2), 83–88. https://doi.org/10.1051/epjap:2003037.
Philipp, A., Lauterborn, W., 1998. Cavitation erosion by single laser-produced bubbles. J. Fluid Mech. 361, 75–116. https://doi.org/10.1017/s0022112098008738.
Pieralli, C., Tribillon, G., 1987. 3d image-processing applied to optical profilometry for the study of the cavitation erosion phenomenon. J. Opt. Nouv. Rev. D. Opt. 18 (1), 9–17. https://doi.org/10.1088/0150-536x/18/1/002.
Plesset, M.S., Chapman, R.B., 1971. Collapse of an initially spherical vapour cavity in neighbourhood of a solid boundary. J. Fluid Mech. 47 (2), 283–290. https://doi.org/10.1017/s0022112071001058.
Prabhakaran, S., Kalainathan, S., Shukla, P., Vasudevan, V.K., 2019. Residual stress, phase, microstructure and mechanical property studies of ultrafine bainitic steel through laser shock peening. Opt. Laser Technol. 115, 447–458. https://doi.org/10.1016/j.optlastec.2019.02.041.
Qin, M., Ju, D.Y., Oba, R., 2006. Improvement on the process capability of water cavitation peening by aeration. Surf. Coat. Technol. 200 (18–19), 5364–5369. https://doi.org/10.1016/j.surfcoat.2005.06.024.
Ramadhan, R.S., Syed, A.K., Tremsin, A.S., Kockelmann, W., Dalgliesh, R., Chen, B., Parfitt, D., Fitzpatrick, M.E., 2018. Mapping residual strain induced by cold working and by laser shock peening using neutron transmission spectroscopy. Mater. Des. 143, 56–64. https://doi.org/10.1016/j.matdes.2018.01.054.
Rawers, J.C., McCune, R.A., Dunning, J.S., 1991. Ultrasound treatment of centrifugally atomized 316 stainless steel powders. Metall. Trans. A 22A, 3025–3033.
Ren, X.D., Wang, J., Yuan, S.Q., Adu-Gyamfi, S., Tong, Y.Q., Zuo, C.Y., Zhang, H.F., 2018. Mechanical effect of laser-induced cavitation bubble of 2A02 alloy. Opt. Laser Technol. 105, 180–184. https://doi.org/10.1016/j.optlastec.2018.02.039.
Saitou, N., Enomoto, K., Kurosawa, K., Morinaka, R., Hayashi, E., Ishikwa, T Yoshimura, T., 2003. Development of water jet peening technique for reactor internal components of nuclear power plant, Journal of Jet Flow Engineering, 20, No. 1 (1), 4–12.
Sanders, D., Soyama, H., De Silva, C., 2021. Use of cavitation abrasive surface finishing to improve the fatigue properties of additive manufactured titanium alloy ti6al4v, SAE Technical Papers 2021–2001-0024, 10.4271/2021–01-0024.
Sano, Y., 2020. Quarter century development of laser peening without coating. Metals 10 (1), 1–11. https://doi.org/10.3390/met10010152.
Sano, Y., Akita, K., Sano, T., 2020. A mechanism for inducing compressive residual stresses on a surface by laser peening without coating. Metals 10 (6), 1–12. https://doi.org/10.3390/met10060816.
Sano, Y., Obata, M., Kubo, T., Mukai, N., Yoda, M., Masaki, K., Ochi, Y., 2006. Retardation of crack initiation and growth in austenitic stainless steels by laser peening without protective coating. Mater. Sci. Eng. A 417 (1–2), 334–340. https://doi.org/10.1016/j.msea.2005.11.017.
Sanchez, A.G., You, C., Leering, M., Glaser, D., Furfari, D., Fitzpatrick, M.E., Wharton, J., Reed, P.A.S., 2021. Effects of laser shock peening on the mechanisms of fatigue short crack initiation and propagation of AA7075-T651. International Journal of Fatigue 143. https://doi.org/10.1016/j.ijfatigue.2020.106025.

Sasaki, T., Yoshida, K., Nakagawa, M., Yoshida, S., 2016. Effect of horn tip geometry on ultrasonic cavitation peening, residual stress, thermomechanics & infrared imaging, hybrid techniques and inverse problems, 9, 139–146.
Sasoh, A., Watanabe, K., Sano, Y., Mukai, N., 2005. Behavior of bubbles induced by the interaction of a laser pulse with a metal plate in water. Appl. Phys. A 80, 1497–1500.
Schiffner, K., Helling, C.D.G., 1999. Simulation of residual stresses by shot peening. Comput. Struct. 72 (1–3), 329–340. https://doi.org/10.1016/s0045-7949(99)00012-7.
Seki, M., Nishie, N., Kozai, S., Kakuda, M., Soyama, H., Naito, A., Fujii, M., 2012. Fatigue strength of steel rollers and gears treated by cavitation peening with short processing time. J. Adv. Mech. Des. Syst. Manuf. 6 (1), 33–43. https://doi.org/10.1299/jamdsm.6.33.
Seki, M., Soyama, H., Fujii, M., Yoshida, A., 2008. Rolling contact fatigue life of cavitation-peened steel gear. Tribology Online 3 (2), 116–121. https://doi.org/10.2474/trol.3.116.
Sekine, Y., Miyamoto, N., Soyama, H., 2008. Improvement of fatigue strength of light metallic materials by cavitation shotless peening, Proceeding of 10th International Conference on Shot Peening 111–115.
Sekine, Y., Soyama, H., 2009. Surface modification of alloy tool steel for forging dies by cavitation peening. Rev. Automot. 30 (4), 393–399.
Sekyi-Ansah, J., Wang, Y., Quaisie, J.K., Li, F.Z., Yu, C., Asamoah, E., Liu, H., 2021. Surface characteristics and cavitation damage in 8090al-li alloy by using cavitation water jet peening processing. Iran. J. Sci. Technol. -Trans. Mech. Eng. 45 (1), 299–309. https://doi.org/10.1007/s40997-020-00401-5.
Shimizu, S., Tanioka, K., Ikegami, N., 1997. Erosion due to ultra-high-speed cavitating jet. J. Jpn. Hydraul. Pneum. Soc. 28 (7), 778–784.
Shukla, P., Shen, X., Allott, R., Ertel, K., Robertson, S., Crookes, R., Wu, H., Zammit, A., Swanson, P., Fitzpatrick, M.E., 2021. Response of silicon nitride ceramics subject to laser shock treatment. Ceram. Int. 47 (24), 34538–34553. https://doi.org/10.1016/j.ceramint.2021.08.369.
Sonde, E., Chaise, T., Boisson, N., Nelias, D., 2018. Modeling of cavitation peening: jet, bubble growth and collapse, micro-jet and residual stresses. J. Mater. Process. Technol. 262, 479–491. https://doi.org/10.1016/j.jmatprotec.2018.07.023.
Soyama, H., 2000. Improvement in fatigue strength of silicon manganese steel sup7 by using a cavitating jet. JSME Int. J., Ser. A 43 (2), 173–178.
Soyama, H., 2004. Introduction of compressive residual stress using a cavitating jet in air. J. Eng. Mater. Technol. 126 (1), 123–128. https://doi.org/10.1115/1.1631434.
Soyama, H., 2006. Improvement of fatigue strength of metallic materials by cavitation shotless peening. Met. Finish. N. 7 (2), 48–51.
Soyama, H., 2007. Improvement of fatigue strength by using cavitating jets in air and water. J. Mater. Sci. 42 (16), 6638–6641. https://doi.org/10.1007/s10853-007-1535-8.
Soyama, H., 2011. Enhancing the aggressive intensity of a cavitating jet by means of the nozzle outlet geometry, Journal of Fluids Engineering, 133, paper No. 101301 (10), 1–11, 10.1115/1.4004905.
Soyama, H., 2013. Effect of nozzle geometry on a standard cavitation erosion test using a cavitating jet. Wear 297 (1–2), 895–902. https://doi.org/10.1016/j.wear.2012.11.008.
Soyama, H., 2014a. Enhancing the aggressive intensity of a cavitating jet by introducing a cavitator and a guide pipe, 9, paper No. 13-00238 J. Fluid Sci. Technol. 1, 1–12. https://doi.org/10.1299/jfst.2014jfst0001.
Soyama, H., 2014b. Surface mechanics design of metallic materials for automotive lightweight technology, Proceedings of 1st International Conference on Modern Auto Technology and Services (MATS 2014) 1–4.
Soyama, H., 2015. Surface mechanics design of metallic materials on mechanical surface treatments Mechanical Engineering Reviews, 2, paper No. 14–00192 (1), 1–20.
Soyama, H., 2017. Key factors and applications of cavitation peening. Int. J. Peen. Sci. Technol. 1 (1), 3–60.
Soyama, H., 2019. Comparison between the improvements made to the fatigue strength of stainless steel by cavitation peening, water jet peening, shot peening and laser peening. J. Mater. Process. Technol. 269, 65–78.
Soyama, H., 2020a. Cavitation peening using pulse laser and submerged water jet to improve fatigue strength of aluminum alloy. J. Mater. Sci. Manuf. Res. SRC/JMSMR/VID/103.
Soyama, H., 2020b. Cavitating jet: a review. Appl. Sci. 10, 1–27. https://doi.org/10.3390/app10207280.
Soyama, H., 2020c. Comparison on improvement of fatigue life of stainless steel between submerged laser peening and water film laser peening, Proceeding of JSMS Annual Meeting paper No. 114.
Soyama, H., 2020d. Comparison between shot peening, cavitation peening and laser peening by observation of crack initiation and crack growth in stainless steel. Metals 10 (63). https://doi.org/10.3390/met10010063, 10.3390/met10010063.
Soyama, H., 2021a. Laser cavitation peening and its application for improving the fatigue strength of welded parts. Metals 11 (4), 1–15. https://doi.org/10.3390/met11040531.
Soyama, H., 2021b. Improvement of fatigue properties of magnesium alloy by cavitation peening using a submerged water jet and a pulsed laser. Met. Finish. N. 22 (6), 56–59.
Soyama, H., Chighizola, C.R., Hill, M.R., 2021a. Effect of compressive residual stress introduced by cavitation peening and shot peening on the improvement of fatigue strength of stainless steel. J. Mater. Process. Technol. 288 (116877), 1–10. https://doi.org/10.1016/j.jmatprotec.2020.116877.
Soyama, H., Kikuchi, T., Nishikawa, M., Takakuwa, O., 2011a. Introduction of compressive residual stress into stainless steel by employing a cavitating jet in air. Surf. Coat. Technol. 205 (10), 3167–3174. https://doi.org/10.1016/j.surfcoat.2010.11.031.
Soyama, H., Kuji, C., Kuriyagawa, T., Chighizola, C.R., Hill, M.R., 2021c. Optimization of residual stress measurement conditions for a 2D method using X-ray diffraction and its application for stainless steel treated by laser cavitation peening. Materials 14 (11), 17. https://doi.org/10.3390/ma14112772.
Soyama, H., Kusaka, T., Saka, M., 2001. Peening by the use of cavitation impacts for the improvement of fatigue strength. J. Mater. Sci. Lett. 20 (13), 1263–1265. https://doi.org/10.1023/a:1010947528358.
Soyama, H., Lichtarowicz, A., 1996. Cavitating jets - similarity correlations. J. Jet. Flow. Eng. 13 (2), 9–19. No. 2.
Soyama, H., Macodiyo, D.O., 2005. Fatigue strength improvement of gears using cavitation shotless peening. Tribology Lett. 18 (2), 181–184. https://doi.org/10.1007/s11249-004-1774-7.
Soyama, H., Macodiyo, D.O., Mall, S., 2004. Compressive residual stress into titanium alloy using cavitation shotless peening method. Tribology Lett. 17 (3), 501–504. https://doi.org/10.1023/B:TRIL.0000044497.45014.f2.
Soyama, H., Miyamoto, N., 2015. Improvement of fatigue strength of light metallic materials by cavitation peening, Proceedings of 1st International Workshop on Cavitation Peening and Related Phenomena 29–30.
Soyama, H., Nagasaka, K., Takakuwa, O., Naito, A., 2012a. Optimum injection pressure of a cavitating jet for introducing compressive residual stress into stainless steel. J. Power Energy Syst. 6 (2), 63–75. https://doi.org/10.1299/jpes.6.63.
Soyama, H., Ohba, K., Takeda, S., Oba, R., 1994. High-speed observations of highly erosive vortex cavitation around butterfly valve. Trans. JSME 60B (572), 1133–1138.
Soyama, H., Okura, Y., 2018. The use of various peening methods to improve the fatigue strength of titanium alloy Ti6Al4V manufactured by electron beam melting, AIMS. Mater. Sci. 5 (5), 1000–1015. https://doi.org/10.3934/matersci.2018.5.1000.
Soyama, H., Park, J.D., Saka, M., 2000. Use of cavitating jet for introducing compressive residual stress. J. Manuf. Sci. Eng. 122 (1), 83–89. https://doi.org/10.1115/1.538911.
Soyama, H., Saito, K., Saka, M., 2002. Improvement of fatigue strength of aluminum alloy by cavitation shotless peening. J. Eng. Mater. Technol. 124 (2), 135–139. https://doi.org/10.1115/1.1447926.
Soyama, H., Sanders, D., 2019. Use of an abrasive water cavitating jet and peening process to improve the fatigue strength of titanium alloy 6Al-4V manufactured by the electron beam powder bed melting (EBPB) additive manufacturing method. JOM 71 (12), 4311–4318.
Soyama, H., Sasaki, K., Saito, K., Saka, M., 2003. Cavitation shotless peening for improvement of fatigue strength of metallic materials. JSAE Trans. 34 (1), 101.
Soyama, H., Sekine, Y., 2010. Sustainable surface modification using cavitation impact for enhancing fatigue strength demonstrated by a power circulating-type gear tester, International Journal of Sustainable Engineering, 3 (1), 25–32, 10.1080/19397030903395174.
Soyama, H., Shimizu, M., Hattori, Y., Nagasawa, Y., 2008. Improving the fatigue strength of the elements of a steel belt for CVT by cavitation shotless peening. J. Mater. Sci. 43 (14), 5028–5030. https://doi.org/10.1007/s10853-008-2743-6.
Soyama, H., Simoncini, M., Cabibbo, M., 2021b. Effect of cavitation peening on fatigue properties in friction stir welded aluminum alloy AA5754. Metals 11 (1), 59. https://doi.org/10.3390/met11010059.
Soyama, H., Takakuwa, O., 2011. Enhancing the aggressive strength of a cavitating jet and its practical application. J. Fluid Sci. Technol. 6 (4), 510–521. https://doi.org/10.1299/jfst.6.510.
Soyama, H., Takakuwa, O. , Naito, A., 2012b. Effect of nozzle shape for high injection pressure on aggressivity of cavitating jet, Proceeding of 21st International Conference on Water Jetting, 367–378.
Soyama, H., Takeo, F., 2020. Effect of various peening methods on the fatigue properties of titanium alloy Ti6Al4V manufactured by direct metal laser sintering and electron beam melting. Materials 13 (10), 2216. https://doi.org/10.3390/ma13102216.
Soyama, H., Yamada, N., 2008. Relieving micro-strain by introducing macro-strain in a polycrystalline metal surface by cavitation shotless peening. Mater. Lett. 62 (20), 3564–3566. https://doi.org/10.1016/j.matlet.2008.03.055.
Soyama, H., Yamauchi, Y., Ikohagi, T., Oba, R., Sato, K., Shindo, T., Oshima, R., 1996. Marked peening effects by highspeed submerged-water-jets - residual stress change on SUS304. J. Jet. Flow. Eng. 13 (1), 25–32.
Sriraman, M.R., Vasudevan, R., 1998. Influence of ultrasonic cavitation on surface residual stresses in AISI304 stainless steel. J. Mater. Sci. 33 (11), 2899–2904. https://doi.org/10.1023/a:1017506424360.
Takahashi, K., Osedo, H., Suzuki, T., Fukuda, S., 2018. Fatigue strength improvement of an aluminum alloy with a crack-like surface defect using shot peening and cavitation peening. Eng. Fract. Mech. 193, 151–161. https://doi.org/10.1016/j.engfracmech.2018.02.013.
Takahashi, N., Kugimiya, T., Seki, T., Terao, K., Kunoh, T., Mizuno, M., 1987. Application of ultrasonic cavitation to metal working and surface-treatment of mild-steel. JSME Int. J. 30 (266), 1229–1236. https://doi.org/10.1299/jsme1987.30.1229.
Takakuwa, O., Nakai, M., Narita, K., Niinomi, M., Hasegawa, K., Soyama, H., 2016a. Enhancing the durability of spinal implant fixture applications made of Ti-6Al-4V eli by means of cavitation peening. Int. J. Fatigue 92, 360–367.
Takakuwa, O., Nishikawa, M., Soyama, H., 2011. Technique for partially strengthening electrical steel sheet of IPM motor using cavitation peening. Mater. Sci. Technol. 27 (9), 1422–1426. https://doi.org/10.1179/026708310×12712410311695.
Takakuwa, O., Takeo, F., Sato, M., Soyama, H., 2016b. Using cavitation peening to enhance the fatigue strength of duralumin plate containing a hole with rounded edges. Surf. Coat. Technol. 307, 200–205.
Takata, T., Enoki, M., Chivavibul, P., Matsui, A., Kobayashi, Y., 2016. Effect of confinement layer on laser ablation and cavitation bubble during laser shock

peening. Mater. Trans. 57 (10), 1776–1783. https://doi.org/10.2320/matertrans.M2016150.
Tan, K.L., Yeo, S.H., 2017. Surface modification of additive manufactured components by ultrasonic cavitation abrasive finishing. Wear 378–379, 90–95. https://doi.org/10.1016/j.wear.2017.02.030.
Tan, Z., Wang, Y., Li, F., Li, R., Yu, C., Fan, H. and Wang, J., 2018a. Numerical simulation of cavitation behavior and peening experiments in cavitation peening processing, Journal of Physics: Conf. Series, 1064 012043, 10.1088/1742–6596/1064/1/012043.
Tan, Z.R., Wang, Y., Li, F.Z., Li, R.T., Yu, C., Fan, H.Y., Wang, J.J. and Iop. (2018b). Numerical simulation of cavitation behavior and peening experiments in cavitation peening processing. In 2018 2nd international conference on fluid mechanics and industrial applications (Vol. 1064). Bristol: IOP Publishing Ltd.
Tanaka, K., Shimonishi, D., Nakagawa, D., Ijiri, M., Yoshimura, T., 2019. Stress relaxation behavior of cavitation-processed Cr-Mo steel and Ni-Cr-Mo steel. Appl. Sci. -Basel 9 (2), 8. https://doi.org/10.3390/app9020299.
Telang, A., Gili, A.S., Mannava, S.R., Qian, D., Vasudevan, V.K., 2018. Effect of temperature on microstructure and residual stresses induced by surface treatments in inconel 718 SPF. Surf. Coat. Technol. 344, 93–101. https://doi.org/10.1016/j.surfcoat.2018.02.094.
Thiruvengadam, A., Preseir, H.S., 1964. On testing materials for cavitation damage resistance. J. Ship Res. 8, 39–56.
Tiwari, B.K., 2015. Ultrasound: a clean, green extraction technology. TrAC Trends Anal. Chem. 71, 100–109. https://doi.org/10.1016/j.trac.2015.04.013.
Toh, C.K., 2007. The use of ultrasonic cavitation peening to improve micro-burr-free surfaces. Int. J. Adv. Manuf. Technol. 31 (7–8), 688–693. https://doi.org/10.1007/s00170-005-0249-9.
Tomota, Y., Ojima, M., Harjo, S., Gong, W., Sato, S., Ungar, T., 2019. Dislocation densities and intergranular stresses of plastically deformed austenitic steels. Mater. Sci. Eng. A 743, 32–39. https://doi.org/10.1016/j.msea.2018.09.052.
Torres, M.A.S., Voorwald, H.J.C., 2002. An evaluation of shot peening, residual stress and stress relaxation on the fatigue life of AISI 4340 steel. Int. J. Fatigue 24 (8), 877–886. https://doi.org/10.1016/s0142-1123(01)00205-5.
Turski, M., Clitheroe, S., Evans, A.D., Rodopoulos, C., Hughes, D.J., Withers, P.J., 2010. Engineering the residual stress state and microstructure of stainless steel with mechanical surface treatments. Appl. Phys. A-Mater. Sci. Process. 99 (3), 549–556. https://doi.org/10.1007/s00339-010-5672-6.
Vazquez, J., Navarro, C., Dominguez, J., 2012. Experimental results in fretting fatigue with shot and laser peened al 7075-T651 specimens. Int. J. Fatigue 40, 143–153. https://doi.org/10.1016/j.ijfatigue.2011.12.014.
Vidvans, A.N., Melkote, S.N., Sanders, D.G., 2021. Enhancing cavitation intensity in co-flow water cavitation peening with organ pipe nozzles. J. Manuf. Sci. Eng. 143 (7), 10. https://doi.org/10.1115/1.4049649.
Wang, B., Castellana, J., Melkote, S.N., 2021a. A hybrid post-processing method for improving the surface quality of additively manufactured metal parts. Cirp Ann. -Manuf. Technol. 70 (1), 175–178. https://doi.org/10.1016/j.cirp.2021.03.010.
Wang, C., Luo, K., Bu, X., Su, Y., Cai, J., Zhang, Q., Lu, J., 2020. Laser shock peening-induced surface gradient stress distribution and extension mechanism in corrosion fatigue life of aisi 420 stainless steel. Corros. Sci. 177. https://doi.org/10.1016/j.corsci.2020.109027.
Wang, C., Luo, K., Wang, J., Lu, J., 2022. Carbide-facilitated nanocrystallization of martensitic laths and carbide deformation in AISI 420 stainless steel during laser shock peening. Int. J. Plast. 150. https://doi.org/10.1016/j.ijplas.2021.103191.
Wang, C.Y., Cheng, W., Shao, Y.K., Luo, K.Y., Lu, J.Z., 2021b. Cavitation erosion behaviour of AISI 420 stainless steel subjected to laser shock peening as a function of the coverage layer in distilled water and water-particle solutions. Wear 470–471. https://doi.org/10.1016/j.wear.2020.203611.
Wu, J.Z., Liu, H.J., Wei, P.T., Lin, Q.J., Zhou, S.S., 2020. Effect of shot peening coverage on residual stress and surface roughness of 18CrNiMo7-6 steel. Int. J. Mech. Sci. 183, 11. https://doi.org/10.1016/j.ijmecsci.2020.105785.
Yamaguchi, A., Shimizu, S., 1987. Erosion due to impingement of cavitating jet. J. Fluids Eng. 109 (4), 442–447.
Yamaguchi, H., Shinmura, T., Kasai, K., Aizawa, T., 2002. Study of micro-machining process applying cavitation based on ultrasonic vibration. Trans. JSME 68 (673), 2777–2782.
Yamauchi, Y., Asami, K., Soyama, H., Sato, K., Ikohagi, T., Oba, R., 1995. Marked effects of ambient pressure on impinging erosion induced by high-speed submerged water jets. Trans. JSME 61B (583), 785–792.
Yamauchi, Y., Soyama, H., Sato, K., Ikohagi, T., Oba, R., 1994. Development of erosion in high-speed submerged water jets. Trans. JSME 60B (571), 736–743.
Yang, Y.F., Shi, W.D., Li, W., Chen, S.P., Zhang, W.Q., Pan, B., 2021. Experimental study on the surface property changes of aluminum alloy and stainless steel after impingement with submerged cavitation jet. Strength Mater. 53 (2), 353–363. https://doi.org/10.1007/s11223-021-00294-y.
Zhang, H., Han, B., Yu, X.G., Ju, D.Y., 2013. Numerical and experimental studies of cavitation behavior in water-jet cavitation peening processing. Shock Vib. 20 (5), 895–905. https://doi.org/10.3233/sav-130792.
Zhang, H.F., Ren, X., Tong, Y.Q., Larson, E.A., Adu-Gyamfi, S., Wang, J., Li, X., 2019. Surface integrity of 2A70 aluminum alloy processed by laser-induced peening and cavitation bubbles. Results Phys. 12, 1204–1211. https://doi.org/10.1016/j.rinp.2018.11.093.
Zhang, Q., Li, H., Zhai, M., Mohsan, A.U.H., Zhao, S., 2021. Numerical and experimental study on the deformation of aluminum alloy ring treated by ultrasonic shot peen forming. Int. J. Adv. Manuf. Technol. 113 (9–10), 2791–2804. https://doi.org/10.1007/s00170-021-06786-0.
Zhang, W.W., Yao, Y.L., Noyan, I.C., 2004. Microscale laser shock peening of thin films, part 1: experiment, modeling and simulation. J. Manuf. Sci. Eng. 126 (1), 10–17. https://doi.org/10.1115/1.1645878.
Zhou, J., Retraint, D., Sun, Z., Kanoute, P., 2018. Comparative study of the effects of surface mechanical attrition treatment and conventional shot peening on low cycle fatigue of a 316L stainless steel. Surf. Coat. Technol. 349, 556–566. https://doi.org/10.1016/j.surfcoat.2018.06.041.